Turun yliopisto
University of Turku

OBSERVATIONAL STUDIES OF CORE-COLLAPSE SUPERNOVA PROGENITORS AND THEIR ENVIRONMENTS

Tuomas Kangas

TURUN YLIOPISTON JULKAISUJA – ANNALES UNIVERSITATIS TURKUENSIS
Sarja – ser. AI osa – tom. 558 | Astronomica – Chemica – Physica – Mathematica | Turku 2017

Turun yliopisto
University of Turku

OBSERVATIONAL STUDIES OF CORE-COLLAPSE SUPERNOVA PROGENITORS AND THEIR ENVIRONMENTS

Tuomas Kangas

TURUN YLIOPISTON JULKAISUJA – ANNALES UNIVERSITATIS TURKUENSIS
Sarja - ser. A I osa - tom. 558 | Astronomica - Chemica - Physica - Mathematica | Turku 2017

University of Turku

Faculty of Mathematics and Natural Sciences
Department of Physics and Astronomy

Supervised by

Seppo Mattila
Professor
Department of Physics and Astronomy
University of Turku
Finland

Jari Kotilainen
Professor
Finnish Centre for Astronomy with ESO
University of Turku
Finland

Reviewed by

Peter Johansson
Associate Professor
Department of Physics
University of Helsinki
Finland

Keiichi Maeda
Associate Professor
Department of Astronomy
Kyoto University
Japan

Opponent

Bruno Leibundgut
VLT Programme Scientist
European Southern Observatory
Germany

The originality of this thesis has been checked in accordance with the University of Turku quality assurance system using the Turnitin OriginalityCheck service.

ISBN 978-951-29-6820-6 (PRINT)
ISBN 978-951-29-6821-3 (PDF)
ISSN 0082-7002 (Print)
ISSN 2343-3175 (Online)
Painosalama Oy - Turku, Finland 2017

Acknowledgements

Among those that helped make this work what it is, the supervisor's influence is first and foremost. I thank my primary supervisor Seppo Mattila for all his effort in coaching and advising me over the past several years, and for always maintaining the optimal balance between distance and availability that let me work in peace or pester him with questions as needed.

I thank my secondary supervisor Jari Kotilainen, who along with Seppo also supervised my MSc thesis, and who originally hired me as an intern at Tuorla Observatory and started me on the path of H α images and supernovae that led me here. I thank Erkki Kankare who, along with Seppo, convinced me to take up a studentship at the Nordic Optical Telescope which led to possibly the best year-and-a-half of my life. I thank the NOT staff and all the other students at NOT and other telescopes on La Palma who helped make it such a good time. I thank the staff at Tuorla for making the working environment at the observatory pleasant.

I thank the pre-examiners Keiichi Maeda and Peter Johansson for thoroughly reading the thesis and supplying valuable comments, and Bruno Leibundgut for agreeing to be my opponent at the thesis defense. I thank the University of Turku Graduate School, the University of Turku foundation and the Emil Aaltonen foundation for their financial support of my PhD thesis work.

In addition to the aforementioned people and organizations, I thank Morgan Fraser, Laura Portinari, Peter Lundqvist, Petri Väisänen, Nadejda Blagorodnova and a whole crowd of others, too numerous to name here, for their valuable collaboration in my past and present projects.

Last but definitely not least, I thank my parents for their patience and moral support. It is they who encouraged and indulged my scientific curiosity, starting at childhood, and their contribution to this work cannot be overestimated.

Contents

Tiivistelmä

Tämä väitöskirja keskittyy supernovien edeltäjätähtien tutkimukseen. Siinä kuvataan erilaisia tapoja selvittää edeltäjätähtien ominaisuuksia painottaen supernovien ympäristöjen käyttöä. Väitöskirjan sisältämissä artikkeleissa näitä erilaisia menetelmiä käytetään erityyppisten supernovien edeltäjätähtien tutkimiseen. Tuloksista voi vetää johtopäätöksiä liittyen tähtien kehityksen teoriaan, erityisesti massiivisten tähtien kehityksen loppuvaiheisiin. Nämä vaiheet, ja varsinkin massanmenetyksen rooli kehityksessä, ovat puutteellisesti tunnettuja.

Artikkelissa I tutkitaan erityyppisten supernovien korrelaatiota niiden emogalaksien tähtiensyntyalueiden emission välillä, erityisesti paljon tähtiä muodostavissa galakseissa. Myös supernovien säteittäisjakaumaa tutkitaan ja verrataan tavallisissa galakseissa räjähtäneisiin supernoviin. Menetelmän tarkentamiseksi artikkelissa II korrelaatiota massiivisten tähtien ja tähtiensyntyalueiden välillä läheisissä galakseissa verrataan aiempiin vastaaviin tuloksiin supernoville. Tyypin II-P supernovien ja punaisten ylijättiläisten välinen yhteyden ja massiivisten pääsarjatähtien jakauman avulla varmistetaan menetelmän paikkansapitävyys, ja systemaattisia virheitä tutkitaan.

Artikkeli III kuvaa vuorovaikuttavan tyypin II-L supernovan SN 2013fc:n yksityiskohtaisen seurannan tuloksia. Supernovan osoitetaan olevan samankaltainen kuin perusteellisesti tutkittu SN 1998S. Räjähdyksen ympäristöön sovitetaan tähtipopulaatiomalleja, ja edeltäjätähden osoitetaan mahdollisesti olevan massiivinen punainen ylijättiläistähti. Artikkeli IV kuvailee tyyin Ic superkirkkaan supernovan Gaia16apd:n seurantaa ja sen tuloksia. Supernovan valokäyrään sovitetaan magnetar-malleja, ja räjähdys on yhteensopiva vastasyntyneen magnetarin hidastumisesta vapautuvan energian kanssa. Se on kehitykseltään hitaasti ja nopeasti kehittyvien tyypin Ic superkirkkaiden supernovien välimuoto ja mahdollisesti merkki siitä, että näiden supernovien edeltäjätähdet ovat samankaltaisia.

Abstract

In this doctoral thesis, core-collapse supernova progenitor stars are studied. Different ways to gain information on the progenitor stars of core-collapse supernovae are explored, with an emphasis on using the environments of supernovae. In the articles included in the thesis, various such methods are demonstrated and utilized to constrain the progenitor stars of different types of supernovae. The results have implications for the theory of stellar evolution, especially the relatively poorly understood evolution of stars massive enough to explode as core-collapse supernovae and, in particular, the role of mass loss in such stars.

In Paper I, the associations between different types of core-collapse supernovae and the emission of their strongly star-forming host galaxies at different wavelengths are studied statistically. The radial distributions of these supernova types are also examined and compared to those in normal galaxies. In Paper II, the associations between different types of massive stars and star-forming regions in nearby galaxies are compared to studies using supernovae in an effort to approach the method quantitatively. The connection between type II-P supernovae and red supergiants, as well as results from massive main-sequence stars, are used to verify the validity of the method, and systematic effects are investigated.

In Paper III, the results of a detailed follow-up programme of the interacting type II-L supernova SN 2013fc are presented. The supernova is found to be similar to the well-studied event SN 1998S. The environment of the event is compared to stellar population models, and the progenitor of SN 2013fc is found to be consistent with a massive red supergiant star. Paper IV describes the follow-up of the type Ic superluminous supernova Gaia16apd. Magnetar fits to the light curve are performed. The event is consistent with being powered by the spin-down of a newborn magnetar, and its spectroscopic and photometric evolution intermediate between fast and slow type Ic superluminous supernovae hints at similar origins for all members of this photometrically diverse class.

List of publications

I Spatial distributions of core-collapse supernovae in infrared-bright galaxies,
T. Kangas, S. Mattila, E. Kankare, J.K. Kotilainen, P. Väisänen, R. Greimel and A. Takalo (2013), MNRAS, 436, 3464 [arXiv:1309.6781]

II Core-collapse supernova progenitor constraints using the spatial distributions of massive stars in local galaxies,
T. Kangas, L. Portinari, S. Mattila, M. Fraser, E. Kankare, R.G. Izzard, P. James, C. González-Fernández, J.R. Maund and A. Thompson (2017), A&A, 597, A92 [arXiv:1608.06097]

III Supernova 2013fc in a circumnuclear ring of a luminous infrared galaxy: the big brother of SN 1998S,
T. Kangas, S. Mattila, E. Kankare, P. Lundqvist, P. Väisänen, M. Childress, G. Pignata, C. McCully, S. Valenti, J. Vinkó, A. Pastorello, N. Elias-Rosa, M. Fraser, A. Gal-Yam, R. Kotak, J.K. Kotilainen, S.J. Smartt, L. Galbany, J. Harmanen, D.A. Howell, C. Inserra, G.H. Marion, R.M. Quimby, J.M. Silverman, T. Szalai, J.C. Wheeler, C. Ashall, S. Benetti, C. Romero-Cañizales, K.W. Smith, M. Sullivan, K. Takáts and D.R. Young (2016), MNRAS, 456, 323 [arXiv:1509.05389]

IV Gaia16apd – a link between fast-and slowly-declining type I superluminous supernovae,
T. Kangas, N. Blagorodnova, S. Mattila, P. Lundqvist, M. Fraser, U. Burgaz, E. Cappellaro, J. M. Carrasco Martínez, N. Elias-Rosa, L. K. Hardy, J. Harmanen, E. Y. Hsiao, E. Kankare, Z. Kołaczkowski, M. B. Nielsen, T. M. Reynolds, L. Rhodes, A. Somero, M. D. Stritzinger, and Ł. Wyrzykowski (2016), MNRAS, accepted [arXiv:1611.10207]

List of abbreviations

AGB	asymptotic giant branch
BSG	blue supergiant
CCSN	core-collapse supernova
CDS	cool dense shell
CSM	circumstellar medium/matter
ECSN	electron-capture supernova
FIR	far-infrared
FWHM	full width at half maximum
GRB	gamma-ray burst
HRD	Hertzsprung-Russell diagram
HST	*Hubble Space Telescope*
IFS	integral field spectroscopy
IFU	integral field unit
IMF	initial mass function
ISM	interstellar medium
LBV	luminous blue variable
LIRG	luminous infrared galaxy
LMC	Large Magellanic Cloud
MS	main sequence
NCR	normalized cumulative rank
NIR	near-infrared
NOT	Nordic Optical Telescope
NUV	near-ultraviolet
PISN	pair-instability supernova
PSF	point spread function
RLOF	Roche-lobe overflow
RSG	red supergiant
SE-SN	stripped-envelope supernova
SLSN	superluminous supernova
SN	supernova
SNR	supernova remnant
TDE	tidal disruption event
ULIRG	ultraluminous infrared galaxy
UV	ultraviolet
WD	white dwarf
WR	Wolf-Rayet
YHG	yellow hypergiant
YSG	yellow supergiant
ZAMS	zero-age main-sequence

Chapter 1

Introduction

Supernova (SN) events have been observed throughout millennia. These transient events were sometimes bright enough to be observed with the naked eye. The earliest recorded SN, observed by the ancient Chinese, dates back to the year 185 – and, using the modern naming convention, is thus known as SN 185. Other significant historical SNe include SN 1006, with the highest reported apparent brightness; SN 1054 which produced the famous Crab Nebula; SN 1572 which, observed by Tycho Brahe, helped dispel the old world cosmological models with their notion of unchanging heavens; and SN 1604, the last SN visually detected in our own galaxy[1]. The first extragalactic SN was discovered in 1885 in the Andromeda galaxy.

Tycho Brahe and others considered SN 1572 to be the appearance of a new star, *nova stella*, in the sky. This impression resulted in the widespread use of the word *nova* to refer to such appearances of temporary star-like objects that lasted weeks or months before fading away. Novae were later distinguished from an intrinsically brighter class of events, called *supernovae*, by Walter Baade and Fritz Zwicky in 1934. Novae were found to be outbursts of white dwarf (WD) stars accreting matter, while the progenitors of the much more energetic SNe were suggested to be the transitions of massive normal stars into extremely dense neutron stars at the ends of their lives in tremendously energetic explosions. New observations of SNe eventually verified this claim. Other types of SNe were also found, caused by e.g. the terminal explosions of WDs in so-called thermonuclear SNe.

Nowadays, new SNe are discovered by the hundreds each year, as several new transient surveys are able to map the entire sky every few days.

[1] Remnants of SNe that occurred later – such as Cassiopeia A – have been discovered, but not the explosions themselves.

New technology allows us to study SNe at ever larger distances and with ever higher cadence. Because of the extreme brightness of SNe, they can be observed over cosmological distances, and the remarkably uniform class of thermonuclear SNe, in particular, has been used as a distance indicator, or 'standard candle'. These SNe were instrumental in discovering the accelerating expansion of the universe and the existence of dark energy, which led to the Nobel Prize in Physics in the year 2011. However, uncertainties still remain in the progenitor scenarios of thermonuclear SNe. The most important question is whether the progenitors of most thermonuclear SNe are single WDs accreting matter from a companion star or merging double WD systems.

Apart from the cosmological uses of thermonuclear SNe, understanding SNe is an important part of understanding stellar evolution. Information about the final stages of a massive star can be gleaned from the light curve evolution and spectral features of a SN. Mass loss before the SN results in a circumstellar medium (CSM), signatures of which can in some cases clearly be seen in the SN. The mutual interaction between stars in a multiple stellar system also has a profound effect on the evolution of the system, and this too can be investigated through SNe. As massive stars are rare to begin with and the time they spend in their final stages relatively very brief, this final part of a massive star's life remains poorly understood. Thus SNe are a potent tool for stellar astrophysics.

Because of the extreme temperatures, densities and radiation fields in SN explosions, SNe are partially responsible for creating elements that cannot be produced through nuclear fusion in stars, namely, all naturally occurring elements heavier than iron. Recently it has been found that mergers of compact neutron stars, remnants of SNe, also play a part in this. As such, SNe also contribute significantly to the chemical evolution of their individual host galaxies and thus of the universe in general. SNe also inject energy and momentum into the interstellar medium (ISM), creating outflows and turbulence, quenching star formation but also triggering it, and thus influencing the dynamical evolution of their host galaxies in a process known as SN feedback. Therefore, understanding not only how SNe work, but also their occurrence rates in galaxies all over the observable universe, can shed light on this field of astronomy as well.

Considering all this, the progenitors of SNe constitute an important and growing field of study in astronomy. Numerous ways exist to study the progenitors; from directly observing them prior to the explosion to statisti-

cal methods that investigate their environments. In Chapter 2, the basics of stellar evolution are first summarized to provide a background for SNe. Chapter 3 deals with different types of SNe and related transients, reviewing our current knowledge of the progenitors of different SNe. Different ways to study the progenitors of core-collapse SNe (CCSNe) are reviewed in Chapter 4, with an emphasis on environmental studies. A summary of the articles included in this thesis constitutes Chapter 5, and finally, in Chapter 6, plans and possibilities for future work in this field are presented.

Chapter 2

Basics of stellar evolution

A detailed examination of the properties and internal physics of stars is well beyond the scope of this thesis. However, the basic terminology and evolutionary sequence are essential for understanding SNe and their progenitor stars. This brief chapter is based on the book *Stellar Structure and Evolution* (Kippenhahn et al. 2012).

Stars are divided into *spectral classes* depending on their effective (surface) temperatures, which determine their intrinsic colors. The sequence from hottest to coolest is O–B–A–F–G–K–M, followed by the even cooler brown dwarfs. O-type stars are blue, with temperatures $T \gtrsim 20000$ K, while red M-type stars have $T \sim 3000$ K. Each class is divided into subclasses 0 to 9 from hotter to cooler. In addition, the luminosity class of the star is expressed with a Roman numeral, with I denoting a supergiant star, II or III a giant star, IV a subgiant star, V a hydrogen-burning *main sequence* (or dwarf) star and VI a fainter subdwarf star. Thus, for example, the Sun is a G2V-type star. A frequently-used tool for illustrating the stellar types is the *Hertzsprung-Russell diagram* (HRD; Figure 2.1), where stars are placed based on their temperature (i.e. spectral class) and luminosity. Most are clustered on the main sequence, corresponding to the region where a star spends most of its life-time while burning hydrogen. An additional sequence for WDs occupies lower luminosities, and luminous, extended giant stars form the giant branch to the upper right of the main sequence. Above the giant branch are the even more luminous supergiant stars. These different types of stars and their evolution are briefly described below.

A star forms through the gravitational collapse of an interstellar gas cloud. As the cloud contracts it fragments into smaller individual clumps, resulting in the roughly simultaneous birth of a cluster of stars or multiple-star systems. Eventually the increasing density of the clump – causing an

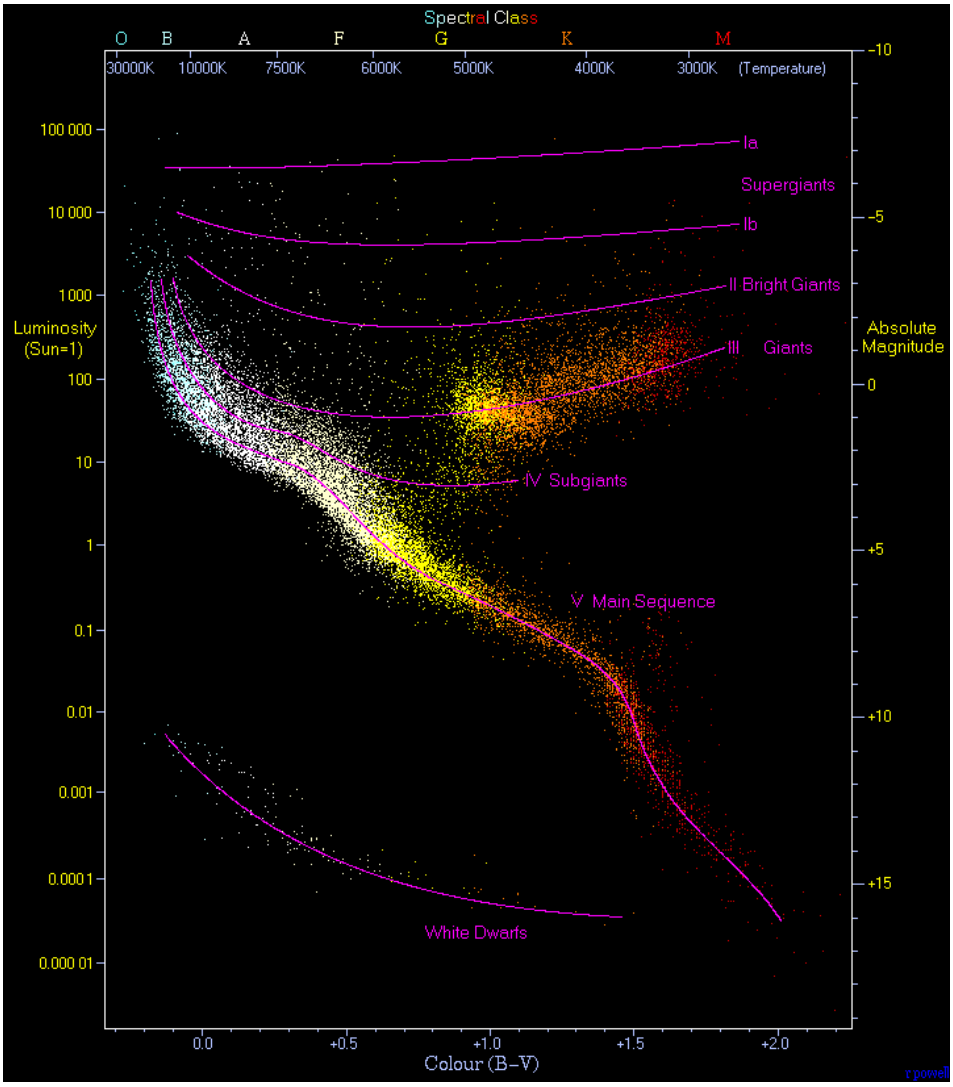

Figure 2.1: An example of a Hertzsprung-Russell diagram, constructed using 22000 stars from the Hipparcos stellar catalog (Perryman et al. 1997). The diagram demonstrates the main sequence and the different branches, and how they relate to spectral classes. Image credited to Richard Powell, used under the Creative Commons license.

increasing opacity and thus optical depth – prevents its thermal energy from escaping through cooling processes, and its temperature increases, slowing the collapse. Until this point the gas is practically in free fall. The free-fall time-scale for a sphere of radius R and mass M is $(\frac{4}{3}\pi R^3)^{\frac{1}{2}}(GM)^{-\frac{1}{2}}$, so for a Solar-mass clump with a typical radius on the order of 10^{15} m, the collapse until this point takes on the order of 10^5 yr. The efficiency of the cooling (via various emission lines) depends on metallicity, and thus the mass of the clump when fragmentation ceases is largest at low metallicity, resulting in more massive stars in the early universe. The dissociation of hydrogen molecules into atoms, and then the ionization of hydrogen and helium, expend energy and re-accelerate the contraction until the object, now called a *protostar*, reaches almost full ionization. From this point it evolves more slowly, contracting as it loses energy through thermal radiation from the surface, moving downward in the HRD. Its core temperature increases until deuterium fusion reactions begin at a few MK, and its luminosity and surface temperature increase. As the core temperature further increases to ∼10 MK and hydrogen fusion begins, the star then settles into the main sequence[1]. The process from the birth of the protostar until the main sequence phase takes a few tens of Myr for a Solar-mass star, but depends heavily on the mass of the protostar: a $15M_\odot$ star, where $M_\odot$ is a Solar mass, only takes tens of thousands of years to reach the main sequence. The massive stars are typically still contracting when the hydrogen fusion starts. Evolution in the main sequence is relatively slow: for example, the luminosity of the Sun has increased by ∼ 30 per cent and its temperature by only a few per cent since the beginning of the main sequence roughly 4.5 Gyr ago.

The mass of a star upon reaching the main sequence is called its zero-age main-sequence (ZAMS) mass or M_{ZAMS}, also called the initial mass. Massive ($M_{\mathrm{ZAMS}} \gtrsim 8M_\odot$) and low-mass ($M_{\mathrm{ZAMS}} \lesssim 8M_\odot$) stars are now examined separately for the purposes of this chapter, as the evolutionary paths of these kinds of stars are quite different. The multiplicity and metallicity of a star also have a significant effect; in the context of SNe, this is covered in Section 3.1.1. A low-mass star, upon entering the main sequence, settles into a long period where its energy source is the fusion of hydrogen into helium. Low-mass stars spend between tens of Myr and tens or even

[1]Brown dwarf stars are not massive enough to reach the temperature required by hydrogen fusion, but are thought to be capable of deuterium burning.

hundreds of Gyr in this stage. This timespan decreases heavily with increasing mass, as a larger mass results in a much higher rate of reactions and a much higher luminosity. The core gradually runs out of hydrogen and is replaced with helium, causing it to contract and its temperature to increase. Hydrogen burning continues in a shell surrounding the core, and the increased temperature (and thus reaction rate) leads to an increased luminosity. The surface of the star expands and cools – it becomes a red giant and moves into the giant branch in the HRD. Eventually the temperature in the helium core is high enough to trigger helium fusion, while the hydrogen-burning shell continues to propagate outward. The onset of helium burning halts the cooling and increase of luminosity, moving the star back down and left in the HRD. As the helium fusion proceeds, this move is reversed again, as the evolution in the HRD is analogous to the previous red giant phase; this is called the asymptotic giant branch (AGB) phase. Helium fusion continues in an outward-moving shell around a carbon-oxygen core, expanding the outer layers of the star – thus lowering the surface gravity, which is proportional to MR^{-2} – and blowing them away in the resulting strong wind[2]. The final product is a WD, a gradually cooling mostly electron-degenerate core supported by the electron degeneracy pressure, composed of carbon, oxygen, neon and/or magnesium, depending on the initial mass of the star. Stars below $\sim 0.5 M_\odot$ never start burning helium or enter the AGB phase, and leave behind helium WDs.

A massive star, on the other hand, undergoes a series of stages of nuclear fusion, from hydrogen through helium, carbon and oxygen to silicon. The contraction of the core at the end of each burning stage raises the temperature enough to trigger the fusion of the next element and stall the gravitational collapse. After the helium-burning phase begins, the outer layers of the star expand and cool, and it moves to the upper right in the HRD, becoming a supergiant star. Stellar winds or interaction with a companion can remove the outer layers of the star, moving it back toward the blue part of the HRD. Depending on their temperature, supergiant stars are divided into *red, yellow or blue supergiants* (RSGs, YSGs or BSGs, respectively). If the star is massive enough ($M_{\mathrm{ZAMS}} \gtrsim 25 M_\odot$) and its mass loss through winds, eruptions or mass transfer to a companion star severe enough, it can lose all its hydrogen and become a *Wolf-Rayet* (WR) star.

[2]Mass loss rates caused by AGB winds can be on the order of $10^{-4} M_\odot$ yr^{-1}, ten orders of magnitude more than the current wind mass-loss rate of the Sun.

The end result of the stages of fusion is iron and other 'iron group' elements, nickel and cobalt, whose binding energy per nucleon is higher than for other elements, and whose fusion into even heavier elements thus does not produce energy. An electron-degenerate iron core develops as the burning of lighter elements proceeds in shells outward from the core. Eventually, as the mass of the core reaches the Chandrasekhar limit of about $1.4M_{\odot}$, it explodes as a SN (see Section 3.1). The lifespan of a massive star is a few to roughly 50 Myr.

The SN explosion typically leaves behind a compact remnant, a *neutron star* or a *black hole*[3]. A neutron star is an extremely dense, neutron-degenerate object whose electrons and protons have combined into neutrons in electron-capture reactions – the mass of the object is on the order of a Solar mass, confined within a radius on the order of 10 km. The nuclear force and the degeneracy pressure of the neutrons are all that keeps it from collapsing further under its own gravity. If it accretes more mass, reaching the Oppenheimer-Volkoff mass of 2 – 3 $M_{\odot}$ (the exact value is not known), nothing can stop its final collapse. A black hole is formed, in its center a singularity, a point of infinite density and spatial curvature, surrounded by an event horizon, the limit past which nothing can escape.

[3]Stars more massive than $\sim 140M_{\odot}$ may explode without leaving any remnant – see Section 3.1.4.

Chapter 3

Supernova types and their progenitors

Broadly speaking, SNe are the terminal explosions of stars that may result in the birth of a neutron star or a black hole or in a complete disruption of the progenitor star. As our ability to observe SNe has improved, the heterogeneity of these events has become more and more apparent, making studies of SN progenitors increasingly important. An illustration of the variety of time-scales and brightnesses of novae, SNe and related transients is shown in Figure 3.1 (Kasliwal 2011). Early on, SNe were separated into two types based on their photospheric spectra by Minkowski (1941): spectra of type I SNe contained no hydrogen features, while those of type II SNe did. These main types were further separated into more and more subtypes, which are described in detail by Filippenko (1997). Type Ia SNe were distinguished from types Ib and Ic based on the presence or absence of a strong Si II line, respectively; type Ib shows helium features while type Ic does not; type II was split into II-P and II-L based on the presence or absence, respectively, of a 'plateau' of nearly constant luminosity until $\sim$ 100 days after the explosion. Some peculiar SNe developed into their own subclasses: type IIn is characterized by narrow emission lines of hydrogen (e.g. Schlegel 1990); type IIb SNe look like type II to begin with but evolve to resemble type Ib SNe (e.g. Filippenko et al. 1993). Even this list proved not to be exhaustive, as new surveys revealed even more subclasses of events such as sub- and superluminous SNe, some of them possibly with wildly different progenitor stars and explosion mechanisms. In this chapter, different transient classes and their proposed physical mechanisms and progenitors are examined, highlighting the remaining open questions in the

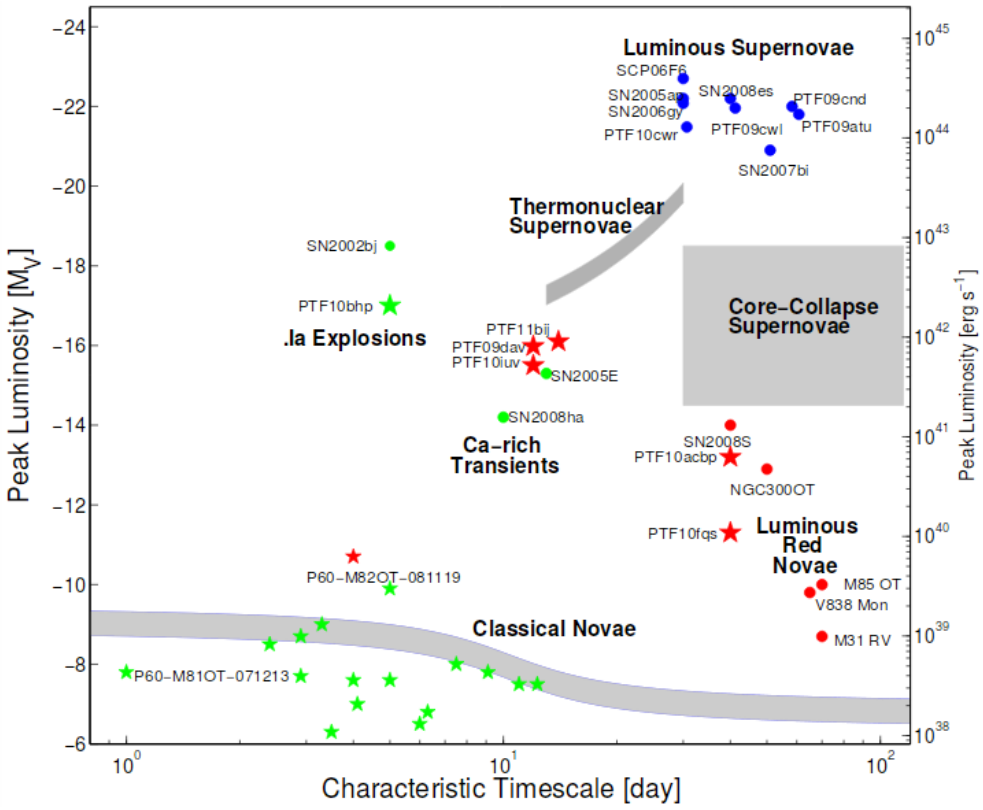

Figure 3.1: Variety of time-scales and brightnesses exhibited by optical transients, including different types of SNe. Adopted from Kasliwal (2011).

field.

3.1 Core-collapse supernovae

Type Ib, Ic and II SNe are together called core-collapse supernovae or CC-SNe. Their progenitors have long been established as ordinary stars at the ends of their lives, typically transitioning into neutron stars (or black holes) in energetic explosions (Baade & Zwicky 1934). Being located in star-forming galaxies but not in elliptical galaxies (van den Bergh & Tammann 1991), their progenitors were assumed to be relatively young and

therefore massive. Nowadays, the prevalent picture of CCSN progenitors is that of stars with $M_{\mathrm{ZAMS}} \geq 8 \pm 1 M_{\odot}$ (Smartt 2009). As explained in Chapter 2, such a star develops an electron-degenerate core composed of iron-group elements. Eventually the mass of the core reaches the Chandrasekhar limit of about $1.4 M_{\odot}$, depending on the exact composition. At this point the electron degeneracy pressure in the core, now unsupported by radiation pressure from fusion reactions, can no longer resist the gravitational force within the core, and the core collapses into a proto-neutron star at a relativistic velocity (see Janka 2007, for a review). Once the nuclear pressure approaches $\rho \approx 10^{14}$ g cm^{-3}, the *neutron* degeneracy pressure can support the structure of the core, and the low compressibility of the proto-neutron star halts the homologous collapse of the outer core. A shock wave is formed and propagates back outward through the core.

From this point on, the exact mechanism of the explosion is somewhat controversial and inadequately understood (Janka 2007). According to the dominant view, the energy of the shock is not sufficient to unbind the star and is spent mostly on the dissociation of heavy nuclei in the outer core. However, the collapse of the core into a neutron star generates an enormous number of neutrinos (mostly from the $e^- + p \rightarrow n + \nu_e$ reaction, but the μ and τ neutrinos are also created), which carry $\sim 10^{53}$ erg[1] of the gravitational potential energy of the star. A small fraction of this energy ($\sim 10^{51}$ erg) is transferred to the outer layers as kinetic energy as some of the neutrinos are reabsorbed. This so-called delayed neutrino heating mechanism possibly works in tandem with the standing accretion shock instability (SASI) mechanism (Blondin et al. 2003), in which non-spherical instabilities develop in the stalled shock and deform it, resulting in asymmetrically enhanced neutrino energy deposition. These processes are believed to revitalize the stalled shock and finally unbind the star, creating the observed SN explosion as the shock breaks out through the surface of the star. Material falling back onto the proto-neutron star can cause a further collapse into a black hole, provided the ZAMS mass of the star is above $\sim 25 M_{\odot}$ (e.g. Fryer 1999). It is also possible that the stalled shock does not receive enough energy to revitalize it, resulting in a failed SN where a star vanishes without an explosion (see also Section 3.4). The characteristic $\sim 10^{51}$ erg of kinetic energy in the SN, contained in the expelled matter called ejecta, is converted into radiation roughly at a 1–10

[1] 1 erg $= 10^{-7}$ J.

per cent efficiency, resulting in total radiated energies of $\sim 10^{49}$ or $\sim 10^{50}$ erg for the common types of CCSNe (Smartt 2009). The conversion happens through shock heating and ionization in the ejecta followed by blackbody radiation and emission in various recombination lines.

Radioactive isotopes of numerous elements are synthesized in the explosion through fusion and neutron capture[2]. The decay of synthesized ^{56}Ni through ^{56}Co into ^{56}Fe is the primary source of energy for the light curve of type I SNe from the shock breakout onwards for hundreds of days (Colgate et al. 1980; Arnett 1982; Barbon et al. 1984). ^{56}Ni and ^{56}Co decay through the electron capture and β^+ processes. The γ photons emitted in this reaction chain and in the annihilation of the emitted positrons have energies in the MeV range, but because of a high optical depth they lose their energy to both free and bound electrons through Compton scattering in the ejecta. The result is a cascade of ionizations and excitations as the freed electrons lose their energy, heating the ejecta through further scatterings. The energy is then re-emitted as blackbody emission peaking in the ultraviolet (UV) or, later, optical range, and through recombination. In type II SNe this decay is masked by other processes, mainly the diffusion of thermal energy deposited by the shock heating (e.g. Grassberg et al. 1971, see also Section 3.1.2), but visible in late phases. The e-folding time, τ, is a parameter used to describe the decay rate of an isotope:

$$\tau = \frac{t_{1/2}}{\ln 2}, \tag{3.1}$$

where $t_{1/2}$ is the half-life of the isotope. The e-folding time for the $^{56}\mathrm{Ni} \rightarrow {}^{56}\mathrm{Co} + \gamma$ reaction is 8.8 days, while for the $^{56}\mathrm{Co} \rightarrow {}^{56}\mathrm{Fe} + \gamma$ reaction it is 111.3 days. Thus the former reaction dominates early on, and the latter from $\sim$ 30 d after maximum brightness (Barbon et al. 1984). The decline of the luminosity of a SN powered by radioactive decay is of the form

$$L(t) = L_0 e^{-t/\tau}, \tag{3.2}$$

where L_0 is the initial luminosity (e.g. Arnett 1982). A change in magnitude

[2]This is the so-called rapid or r-process, where the density of free neutrons is so high that radioactive decay from neutrons to protons is typically not possible before a new neutron capture occurs, resulting in unstable neutron-rich nuclei. The slower s-process, where the decay timescale is shorter than the time between neutron captures, occurs in e.g. AGB stars.

Δm corresponds to a change of luminosity as

$$\Delta m = m - m_0 = -2.5 \log \frac{L}{L_0}, \tag{3.3}$$

where m_0 is the initial magnitude corresponding to L_0. Therefore, assuming complete trapping of the γ rays and positrons by the ejecta, the decline of a SN powered by the decay of ^{56}Co is linear (in magnitudes) with a rate of 0.976 mag / 100 d. The phase of the light curve where ^{56}Co decay is responsible for the luminosity is usually referred to as the *tail phase*. The tail-phase luminosity can be used to estimate the amount of ^{56}Ni synthesized in a SN when complete γ-ray and positron trapping is assumed. This is often done by comparing it to the tail phase of the well-studied SN 1987A, whose light curve in the tail phase adhered to theoretical expectations of ^{56}Co decay with 0.069 $M_\odot$ of synthesized ^{56}Ni (e.g. Bouchet et al. 1991). The assumption of complete trapping is not always valid, however[3], and the actual decline rates during the tail phase can differ from the theoretical value even when other power sources such as interaction with the CSM are not important. The light curves typical to each CCSN type are presented below in their own subsections. Typically the light curve of a SN is divided into two phases. In the *photospheric* phase, a dense and thus optically thick ejecta reprocesses the emission from the inside, which results in a photosphere gradually receding through the expanding ejecta, and the spectrum of the SN is close to a blackbody. The duration of this phase is on the order of 100 days. In the *nebular* phase the ejecta has become optically thin and continuum emission is weak or nonexistent. Nebular-phase emission originates in spectral emission lines in the expanding ejecta. Figure 3.2 demonstrates typical photospheric-phase spectra and Figure 3.3 the light curves of different CCSN types.

The properties of a CCSN depend heavily on the stellar evolution prior to the explosion. Mass loss – whether through eruptions, winds or mass transfer to a companion star – is one of the primary factors in determining the state of a star immediately prior to its death and thus the type of a CCSN; this in turn is influenced by metallicity, rotation, the presence and mass of a binary companion and the ZAMS mass of the progenitor star

[3]The assumption is valid when the optical depth for γ-ray absorption $\tau_\gamma \gtrsim 1$, corresponding to densities of a few $\times 10^{-15}$ g cm^{-3}. The time until γ rays are no longer efficiently trapped depends on ejecta mass and velocity; for example, it is $\sim$ 100 d in type Ic SNe and was $\sim$ 500 d for SN 1987A.

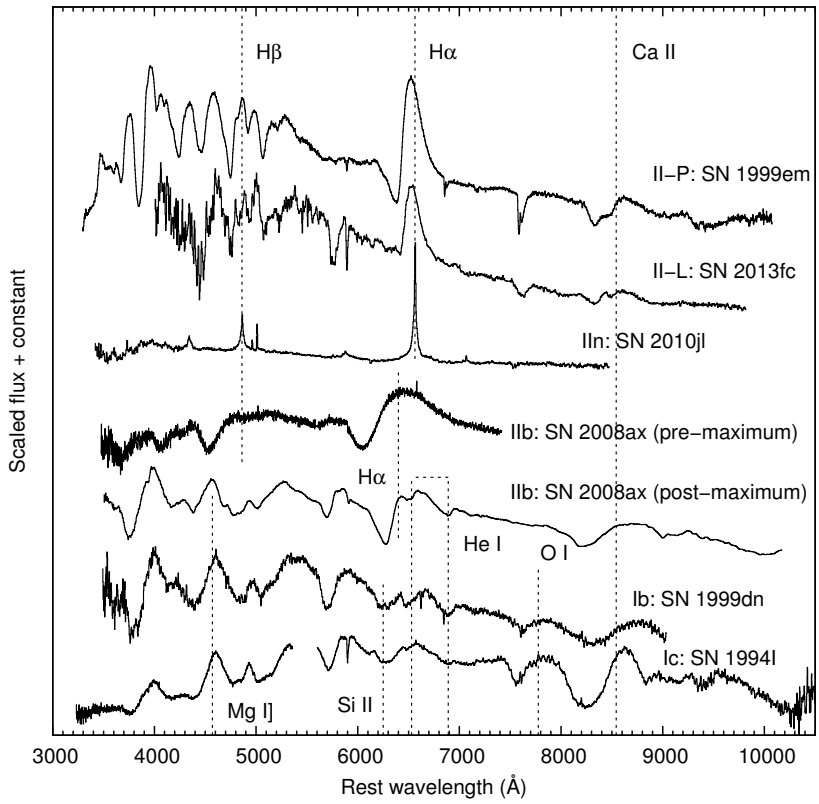

Figure 3.2: Photospheric-phase spectra of example CCSNe of the common types with some prominent spectral lines identified: SN 1999em (type II-P; Hamuy et al. 2001), SN 2013fc (type II-L; Paper III), SN 2010jl (type IIn; Zhang et al. 2012), SN 2008ax (type IIb; Pastorello et al. 2008a; Modjaz et al. 2014), SN 1999dn (type Ib; Benetti et al. 2011) and SN 1994I (type Ic; Filippenko et al. 1995).

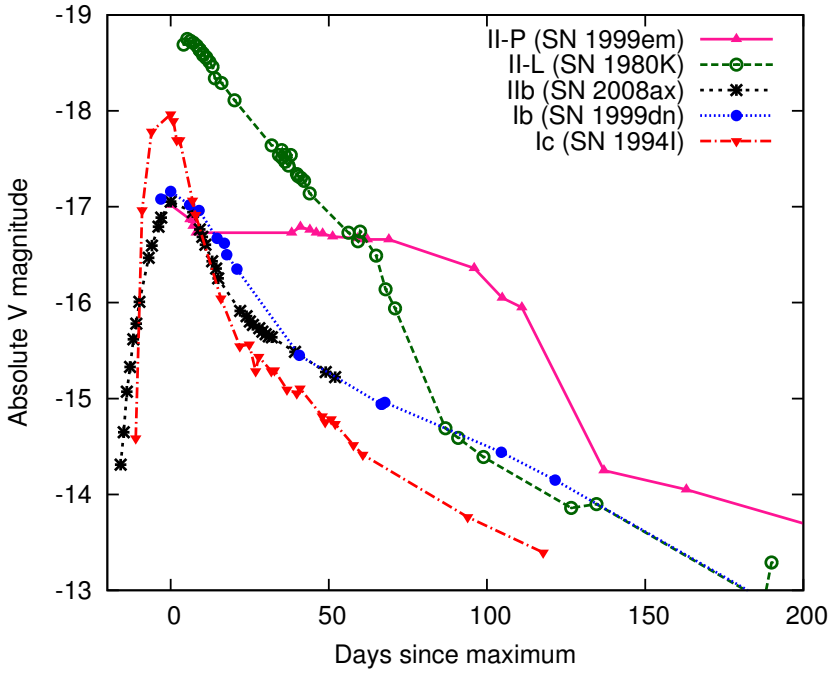

Figure 3.3: Light curves of example CCSNe of the common types: SN 1999em (type II-P; Elmhamdi et al. 2003), SN 1980K (type II-L; Barbon et al. 1982; Buta 1982), SN 2008ax (type IIb; Pastorello et al. 2008a), SN 1999dn (type Ib; Benetti et al. 2011) and SN 1994I (type Ic; Richmond et al. 1996). Type IIn is not shown here, as SNe of this type lack a common light curve shape.

Table 3.1: Relative CCSN rates from Shivvers et al. (2016a). Types II-P and II-L have been combined. Fractions are in per cent.

All CCSNe						
SN type	II				Ib/c+IIb	
Fraction	69.6 ± 6.7				30.4 ± 5.0	
Types Ib/c+IIb						
SN type	IIb	IIb-pec	Ib	Ib-pec	Ic	Ic-BL
Fraction	32.4 ± 10.8	$3.6^{+2.9}_{-3.6}$	37.1 ± 11.7	1.6 ± 1.6	21.3 ± 8.6	$3.9^{+3.0}_{-3.9}$
Type II						
SN type	II		87A-like		IIn	
Fraction	89.1 ± 10.8		$4.2^{+2.4}_{-2.7}$		$6.7^{+3.0}_{-2.9}$	

(Smith 2014). Another consequence of mass loss is the possible presence of a CSM massive enough to considerably influence the evolution of the SN through interaction (e.g. Schlegel 1990; Wang et al. 2004; Pastorello et al. 2008b). The differences between types of CCSNe can be traced to these properties. The types of CCSNe, their observational properties and the corresponding progenitor scenarios are summarized below. Table 3.1 lists the relative rates of different CCSN types (Shivvers et al. 2016a). Observational methods that have been used to study progenitors of CCSNe are examined in more detail in Chapter 4.

3.1.1 Hydrogen-poor CCSNe

Type Ib, Ic and IIb SNe have weak or no hydrogen features in their spectra (e.g. Filippenko 1997). Distinguishing between types Ib and Ic can sometimes be difficult, resulting in some SNe being classified as type Ib/c; types Ib and Ic together are also referred to as Ib/c. Collectively, these three types are also called stripped-envelope SNe (SE-SNe), as the lack of hydrogen in the spectrum indicates that the outer hydrogen-rich layers of the star have been lost prior to the explosion through some mechanism. The nature of this mechanism is still a subject of debate (e.g. Smith 2014, and references therein), with Roche-lobe overflow (RLOF) in an interact-

ing close binary star system and line-driven winds in massive evolved stars (see below) being the leading candidates. This highlights the importance of understanding mass loss processes in the evolution of massive stars.

The vast majority, at least 80 per cent, of O- and B-type stars are located in multiple systems (Kobulnicky & Fryer 2007), with about 70 per cent of all O-type stars expected to interact with a companion and exchange mass when one of the stars expands outside its Roche lobe (Sana et al. 2012). The stars may also enter a common-envelope phase where both of them expand beyond their Roche lobes, and 20 or 30 per cent of O-type stars are expected to merge with a binary companion during their life-times. de Mink et al. (2014) further found that less than a quarter of all massive stars observable at any given time, assuming constant star formation, should be effectively single (i.e. too far from any possible companion to interact). Out of all *apparently* single (radial velocity fluctuations of < 10 km s^{-1}) massive stars, roughly half should either be products of mass transfer and/or merger, or simply pre-mass-transfer binaries too far separated to detect through radial velocity measurements. Figure 3.4 demonstrates the statistics of such a simulated stellar population. Mass transfer rates can be on the order of $10^{-3} M_{\odot}$ yr^{-1} or even more over $\sim 10^4$ yr (Smith 2014). It is clear that binary interaction plays a very significant role in the evolution of massive stars. Paczyński (1967) already suggested that mass loss through RLOF could make a WR star out of a massive star in a binary system, and that this WR star could then explode as a SN. Binary evolution introduces new parameters and complexity, and simplifying assumptions have to be made to reduce the required computing power (Langer 2012). Using such binary codes, Podsiadlowski et al. (1992) argued that both type Ib SNe from exploding helium stars and peculiar type II SNe from post-merger BSGs could result from binary interaction. Numerous later studies (e.g. Eldridge et al. 2008) have also favored binary stars as progenitors of SE-SNe. The ZAMS mass range of such progenitors could stretch as low as 8 $M_{\odot}$.

Another progenitor scenario, for many years the widely favored one, for SE-SNe is that of massive WR stars (with $M_{\mathrm{ZAMS}} \gtrsim 25 M_{\odot}$; Crowther 2007) that have lost their envelopes through strong winds (e.g. Maeder 1981; Gaskell et al. 1986), which are typically on the order of 10^{-5} to $10^{-4} M_{\odot}$ yr^{-1} in massive post-main-sequence stars (Smith 2014). The winds are caused by the transfer of momentum from photons to the stellar atmosphere through absorption and scattering by metal lines in the UV range.

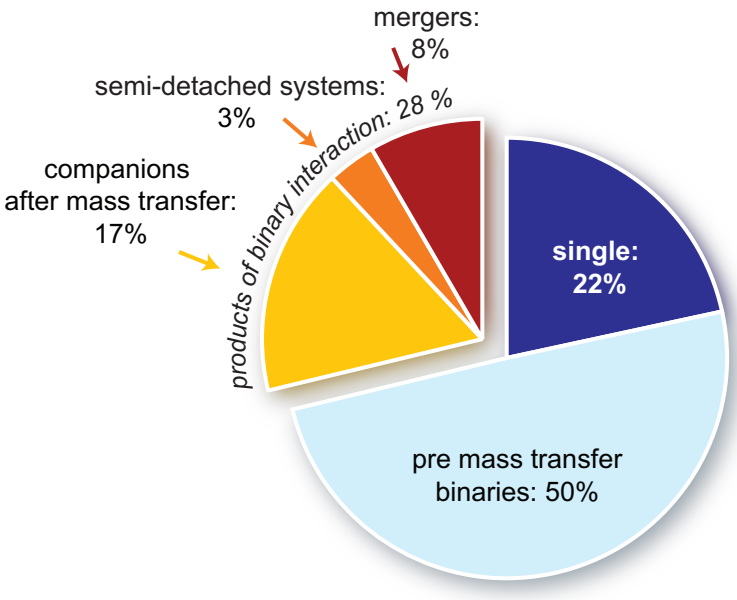

Figure 3.4: Statistics of simulated stellar populations from de Mink et al. (2014), showing the fractions of effectively single stars (i.e. stars without any interaction with a companion), products of binary interaction and pre-mass-transfer binary systems among massive stars ($\gtrsim 8M_{\odot}$) at any given time, assuming continuous star formation. The pre-mass-transfer systems will eventually interact or merge. Semi-detached systems are currently undergoing RLOF.

As such they are referred to as *line-driven winds*. A photon coming from inside the star is absorbed and re-emitted in a random direction, causing a net momentum outwards. The strength of the wind depends on the radiative acceleration over all relevant lines, which in turn depends on the luminosity of the star (and thus temperature); and on the optical depths of the metal lines, which depend on metallicity. A higher metallicity increases the optical depth and thus the mass loss rate – for example, Vink et al. (2001) predict a $\frac{dM}{dt} \propto Z^{0.69}$ or $\frac{dM}{dt} \propto Z^{0.64}$ dependence for stars with $T \gtrsim 25000$ K and $T \lesssim 25000$ K respectively. The metallicity dependence changes with temperature, as the ionization state of the outer envelope (and thus the available lines) depends on temperature. The radiative acceleration is opposed by surface gravity, so an extended star such as an AGB or RSG star loses mass faster. The full physics behind line-driven winds is very complicated, and calculating the actual mass-loss rates requires detailed models incorporating opacities at individual lines that depend on temperature and abundances. A result of the full treatment, a commonly used theoretical recipe (in this case, for $T \gtrsim 25000$ K) by Vink et al. (2001) is

$$\begin{aligned}\log \frac{dM}{dt} &= -6.697 \pm 0.061 + (2.194 \pm 0.021)\log(L/10^5) \\ &\quad - (1.313 \pm 0.046)\log(M/30) - (1.226 \pm 0.037)\log\frac{v_\infty/v_{esc}}{2.0} \\ &\quad + (0.933 \pm 0.064)\log(T/40000) - (10.92 \pm 0.90)[\log(T/40000)]^2 \\ &\quad + (0.85 \pm 0.10)\log(Z/Z_\odot), \end{aligned} \tag{3.4}$$

where v_∞ is the terminal velocity of the wind, v_{esc} the photospheric escape velocity and $Z_\odot$ is Solar metallicity. The unit of $\log \frac{dM}{dt}$ is $M_\odot$ yr^{-1}, L and M are in Solar units and T is in K. This means that roughly speaking, $\frac{dM}{dt} \propto L^{2.2}M^{-1.3}T(v_\infty/v_{esc})^{-1.2}Z^{0.85}$. The total $\frac{dM}{dt} \propto Z^{0.69}$ dependence is due to v_∞ also depending on metallicity.

However, Smith (2014) pointed out that, according to recent studies (e.g. Sundqvist & Owocki 2013), clumping in the wind causes stronger line emission compared to a homogeneous wind, and since emission lines are used as wind mass loss indicators, this leads to overestimated mass loss rates by a factor of about three. Wind mass loss rates that are adjusted for clumping cannot easily lead to single WR stars. Furthermore, the rates of type Ib and Ic SNe relative to other types seem too high to be produced predominantly through wind mass loss in WR stars (Eldridge et al. 2008).

Because of these caveats in the line-driven winds scenario and because of mounting observational evidence, the RLOF mechanism has gained popularity in recent years, and SE-SN progenitors are now believed to be mostly lower-mass interacting binaries, with a possible smaller contribution from massive WR stars (e.g. Papers I and II, Smartt 2009; Anderson et al. 2012; Eldridge et al. 2013; Lyman et al. 2016). However, RLOF is expected to leave a small fraction of the hydrogen envelope behind (Eldridge et al. 2013), indicating that winds should still play a role *in addition to* RLOF in order to produce SE-SNe (except type IIb SNe, which still have a small amount of hydrogen left; see below) and thus metallicity may influence the pre-SN evolution after the RLOF or common-envelope phase (Yoon et al. 2017).

The spectra of type Ib SNe contain prominent features of helium, but lack the silicon features typical to type Ia SNe (see Section 3.2) – for example events, see Benetti et al. (2011), Cao et al. (2013) and Roy et al. (2013), to name only a few. Their light curves correspond to the ^{56}Ni-powered Arnett (1982) model:

$$L(t) = e^{-(\frac{t}{\tau_m})^2} \int_0^{\frac{t}{\tau_m}} P(t') 2 \frac{t'}{\tau_m} e^{(\frac{t'}{\tau_m})^2} \frac{dt'}{\tau_m}, \tag{3.5}$$

where $L(t)$ is luminosity, τ_m is the diffusion time-scale and $P(t)$ is the total power absorbed by the ejecta – in this case provided by ^{56}Ni decay. Type Ib SNe, on average, reach a B-band peak absolute magnitude of -17.5 ± 0.4 mag (Richardson et al. 2014). Although WR progenitors are still favored by a minority (e.g. Groh et al. 2013a), accumulating observational evidence, especially in recent years, largely disfavors massive WR stars as the progenitors of type Ib SNe. Instead, using a direct progenitor detection of the type Ib event iPTF13bvn, ejecta masses, SN rate studies and environmental methods (e.g. Papers I and II, Smith et al. 2011a; Anderson et al. 2012; Kuncarayakti et al. 2015; Eldridge & Maund 2016; Folatelli et al. 2016; Lyman et al. 2016; Shivvers et al. 2016a) the progenitors have been found consistent with interacting binaries with $M_{\mathrm{ZAMS}} \lesssim 20 M_{\odot}$.

Type Ic SNe are characterised by a lack of helium as well as hydrogen in their spectra. Typical features in the spectra include emission and absorption lines of oxygen, calcium and magnesium. For well-studied examples, see e.g. Filippenko et al. (1995), Richmond et al. (1996) and Chen et al. (2014). Type Ic light curves are very similar to type Ib, powered by ^{56}Ni

decay, with an average B-band peak absolute magnitude -17.7 ± 0.4 mag (Richardson et al. 2014). The environments of type Ic SNe exhibit higher metallicities than those of type Ib (Kuncarayakti et al. 2013a), hinting at more powerful line-driven winds contributing to the stronger mass loss prior to the explosion. Their native stellar populations are also younger, which indicates more massive progenitors (e.g. Papers I and II, Anderson et al. 2012; Kuncarayakti et al. 2013a). There is observational evidence for both massive WR stars (van Dyk et al. 2016; Galbany et al. 2016; Maund et al. 2016; Taddia et al. 2016) and interacting binaries (Chen et al. 2014) as the progenitors, with some ambiguous cases such as SN 2002ap (Crockett 2007); the progenitor population of type Ic may well be a combination of both (e.g. Paper II). In any case, their progenitors seem to be more massive than those of type Ib SNe.

A subset of type Ic SNe (roughly 15 per cent; Shivvers et al. 2016a) exhibits spectral lines broader than in normal type Ic SNe, indicating bulk ejecta velocities of roughly 15000 – 30000 km s^{-1}, and are called broad-lined type Ic or Ic-BL SNe, also known as hypernovae. Some type Ic-BL SNe are connected with long-duration (≥ 2 s) gamma-ray bursts (GRBs), and all SNe accompanied by a GRB belong to this type (Milisavljevic et al. 2015); the first discovered SN associated with a GRB was SN 1998bw (e.g. Iwamoto et al. 1998). The host galaxies of type Ic-BL SNe (and GRBs) are faint and exhibit low metallicities compared to other SNe (e.g. Savaglio et al. 2009). Whereas a normal type Ic SN has a kinetic energy close to 10^{51} erg, the kinetic energies of type Ic-BL SNe are 10^{52} erg or more (Nomoto et al. 2001). The high velocities, as well as the accompanying GRB and its afterglow, are believed to be caused by a relativistic jet launched by a central engine, breaking out of the stellar envelope (e.g. Piran 2004). The engine may be accretion onto a black hole formed in a core collapse, or perhaps the spin-down of a millisecond magnetar (for more details on the magnetar scenario, see Sect. 3.1.4). The reason why some type Ic-BL SNe are associated with GRBs and some are not is still an open question – the easiest explanation, that the GRB jet is simply off-axis, has been ruled out by Soderberg et al. (2006). It is possible that the central engine is too weak in some events for the jet to breach the stellar envelope, but still strong enough to accelerate a part of the ejecta to relativistic velocities (Milisavljevic et al. 2015). The events without an associated GRB tend to be less energetic and less luminous, and have a smaller estimated ejecta mass, than the ones that do accompany GRBs (Nomoto et al. 2007). They

are also generally located in higher-metallicity environments (Modjaz et al. 2008), consistently with the notion that a low metallicity is necessary for GRBs.

Type IIb SNe are characterised by spectra that resemble hydrogen-rich type II SNe at first, then evolve to resemble type Ib (e.g. Filippenko et al. 1993) as the Balmer series features disappear. The average B-band peak absolute magnitude of this type is -17.0 ± 0.5 mag (Richardson et al. 2014). Apart from a sharp and narrow secondary maximum before the broader main peak in some cases such as the prototypical type IIb SN 1993J (e.g. Okyudo et al. 1993), the light curve is similar to type I SNe. The photometric and spectroscopic properties, including the narrow initial peak, have been found consistent with the explosion of a supergiant star with most, but not all, of its hydrogen envelope stripped (e.g. Podsiadlowski et al. 1993; Shigeyama et al. 1994; Ergon et al. 2014). The spectroscopic evolution is caused by the photosphere receding through the ejecta as it becomes optically thinner: hydrogen features from the envelope appear at first, but the low hydrogen mass causes the photosphere to quickly reach the helium layer. The initial peak has been interpreted as being caused by the shock breaking out of an extended supergiant progenitor, and its absence has been suggested to be due to a less extended progenitor star (e.g. Pastorello et al. 2008a; Nakar & Piro 2014). The detected progenitors of type IIb SNe have been YSGs or perhaps BSGs in a ZAMS mass range of 13 – 19 $M_{\odot}$, generally in interacting binaries (e.g. Aldering et al. 1994; Maund et al. 2004; van Dyk et al. 2011; Folatelli et al. 2015; Tartaglia et al. 2016c). Other recent studies of type IIb SN progenitors are also consistent with this mass range (e.g. Paper II, Shivvers et al. 2013; Jerkstrand et al. 2015). The binary evolution would also produce the small remaining hydrogen envelopes that type IIb SNe require (Eldridge et al. 2013). Types IIb and Ib may form a continuum where the SN type is determined by whether the final layer of hydrogen is stripped by winds after the RLOF phase (Yoon et al. 2017).

3.1.2 Hydrogen-rich CCSNe

Type II, or hydrogen-rich, SNe still retain a part of their hydrogen envelopes, meaning that they have not been affected by mass loss as strongly as SE-SNe. Thus their spectra exhibit strong hydrogen features, often in the form of a line profile with a combination of emission and blueshifted ab-

sorption, called a *P Cygni profile* (e.g. de Vaucouleurs et al. 1981; Elmhamdi et al. 2003; Hendry et al. 2006). Type IIb SNe, while technically a subtype under type II, have been described in Sect. 3.1.1, but in their early phases their spectra resemble other type II SNe as well. Type II SNe are commonly separated into subtypes II-P ('plateau'), defined by a phase of nearly constant luminosity lasting ~ 100 d followed by a sharp decline into the tail phase, and II-L ('linear'), defined by a linear brightness decline and a short or nonexistent plateau phase (Barbon et al. 1979). Type II-L SNe tend to be brighter (average B-band peak magnitudes -16.8 ± 1.0 for II-P and -18.0 ± 0.4 for II-L; Richardson et al. 2014) – some type II-L events even reach magnitudes brighter than -20 mag (Paper III, de Vaucouleurs et al. 1981). Additionally, the absorption components in the Balmer lines of their spectra are generally weak or nonexistent (Schlegel 1996).

Type II SNe comprise almost 70 per cent of all CCSNe (Shivvers et al. 2016a), even without type IIb SNe included. Most detected SN progenitor stars are those of type II-P SNe (Smartt 2009), making type II-P in particular well understood compared to other types of CCSNe. The progenitors of type II-P SNe have been firmly established as RSG stars with masses between ~ 9 and $\sim 17 M_\odot$ (e.g. Smartt 2009, 2015). The evolution of a type II-P SN can be explained as follows (e.g. Grassberg et al. 1971). The shock wave ionizes the ejecta, drastically increasing its opacity, and the photosphere at early phases is in the outer part of the ejecta. The P Cygni shape of the Balmer lines is due to recombination emission from the ejecta close to the photosphere and absorption in the already-recombined, faster-moving ejecta further out. As the ejecta expands and cools, the inner parts of the ejecta gradually reach the recombination temperature of ~ 6000 K, and the photosphere moves inward as the outer layers recombine and their opacity decreases. This recombination 'wave' receding inward in the ejecta roughly balances the expansion, and the resulting roughly constant temperature and radius of the photosphere power the plateau in the light curve. The following sharp drop in brightness is caused by the recombination wave reaching the helium layer, where recombination has already happened, and the photosphere recedes more quickly until the nebular phase is reached. From that point, the decline rate follows the ^{56}Co decay.

Recently, the separation between types II-P and II-L has been subject to debate (e.g. Arcavi et al. 2012; Anderson et al. 2014; Faran et al. 2014; Sanders et al. 2015), with some recent studies favoring a continuum of properties between the two, and Anderson et al. (2014) drawing the con-

clusion that these subtypes should not exist at all. Some type II-P or II-L SNe have a visible but short 'plateau' phase followed by a drop (usually a modest one) to the tail phase (e.g. Paper III, Valenti et al. 2015), while some type II-P SNe also exhibit II-L-like properties (e.g. Mauerhan et al. 2016). Very few type II-L SNe keep evolving linearly until the tail phase (Anderson et al. 2014). This has been interpreted as a continuum of hydrogen envelope masses, with smaller envelopes not being able to power the plateau for a long time. The brightnesses of type II SNe also seem to form a continuum, with type II-L occupying the higher luminosities (Anderson et al. 2014; Sanders et al. 2015). These factors and the relative rarity of type II-L SNe ($9.7^{+4.0}_{-3.2}$ per cent of all type II SNe according to Li et al. 2011a) hint at higher masses for their RSG progenitors than those of type II-P. Faran et al. (2014) suggest ZAMS masses around 15 $M_\odot$, while the only detected progenitor of a type II-L event, SN 2009hd, had a ZAMS mass of $\lesssim 20M_\odot$ (Elias-Rosa et al. 2011). A higher ZAMS mass would result in stronger mass loss and thus a smaller remaining hydrogen mass. Even more stripping could lead to type IIb SNe, whose progenitors have been found to have about the same ZAMS mass range as type II-L (e.g. Paper II, Jerkstrand et al. 2015).

The best-studied SN in the history of astronomy is SN 1987A, which exploded in the Large Magellanic Cloud (LMC) (e.g. Woosley et al. 1987), and whose identified progenitor was a BSG with a mass of $\sim 20M_\odot$ (Walborn et al. 1987). This star may have been the result of a merger between two stars with masses 5 and 15 $M_\odot$ (Morris & Podsiadlowski 2009). The SN itself, however, was very peculiar, with an initial fast peak followed by a very slow rise to a second peak and a tail phase consistent with ^{56}Co decay (e.g. Bouchet et al. 1991). The CSM around the SN remnant (SNR) shows a distinctive hourglass structure, which could have been produced during the interaction of the pre-merger stars (Morris & Podsiadlowski 2009), but its formation mechanism remains uncertain (McCray & Fransson 2016). A neutrino detection from SN 1987A (e.g. Aglietta et al. 1987) confirmed the neutrino-powered shock in the core collapse explosion scenario. Spectroscopically, the evolution of SN 1987A was slow, with strong P Cygni features typical to type II SNe (e.g. Catchpole et al. 1987; Menzies et al. 1987). SNe similar to SN 1987A are quite rare (as of 2016, 18 have been detected; McCray & Fransson 2016), relatively faint with a mean B-band peak absolute magnitude of -15.1 ± 0.4 (Pastorello et al. 2012) and tend to favor low-metallicity environments (Taddia et al. 2013a). The progenitors

of these rare SNe seem to generally be BSGs around $20M_{\odot}$ (e.g. Pastorello et al. 2012; Takáts et al. 2016).

Kuncarayakti et al. (2013b) argued that some type II SN progenitors may have $M_{\mathrm{ZAMS}} \gtrsim 25M_{\odot}$, and based on the type II-L SN rate, Li et al. (2011a) favored a ZAMS mass range of 18 – 23 $M_{\odot}$. However, for the most part, there seems to be a lack of RSG progenitors with $M_{\mathrm{ZAMS}} \gtrsim 18M_{\odot}$ compared to the initial mass function (IMF) of stars (e.g. Smartt 2009, 2015). This has been called the 'red supergiant problem'. This apparent lack of high-mass RSGs exploding as SNe can be explained in various ways: the RSGs with $M_{\mathrm{ZAMS}} \gtrsim 18M_{\odot}$ may collapse directly into black holes as failed SNe (see Sect. 3.4); they may evolve into other bluer stellar types (BSGs, YSGs or WR stars) before exploding; or they could be highly extinguished by dust in the CSM, resulting in biased mass estimates. Smartt (2015) argued that failed SNe are the most likely explanation, as recent evidence suggests that most type Ib/c SN progenitors are interacting binaries in the 8 – 20 $M_{\odot}$ ZAMS mass range instead of classical WR stars with higher ZAMS masses, and they found no evidence for biases caused by extinction in their mass estimation. However, Beasor & Davies (2016) did find more luminous RSGs in one particular cluster to be more reddened, casting doubt on the latter point. The existence and rates of failed SNe still require observational evidence (e.g. Reynolds et al. 2015), and the 'red supergiant problem' remains an open question with no final answer.

3.1.3 Interaction with CSM

Various subtypes of CCSNe show signs of interaction with their surrounding CSM. Technically, all CCSNe interact with CSM, as stellar wind is present in all massive stars to some extent. However, here only those SNe are considered where the interaction provides a significant early power source through the conversion of kinetic energy into radiation – in addition to, or instead of, internal heating or the shock-deposited energy in a SN ejecta. At very late times (years after the explosion), interaction can take place far from the initial SN, as is happening in the SNR of SN 1987A, where the ejecta-CSM interaction is in the process of destroying the main ring of CSM (Fransson et al. 2015; McCray & Fransson 2016).

The most common interacting CCSNe are of type IIn ('narrow') (Schlegel 1990). SNe of this type exhibit narrow spectral emission lines of hydrogen, originating from the recombination of hydrogen in slowly-moving CSM

shells or winds around the progenitor star. The hydrogen is photoionized by the initial flash of the SN. This, however, is the only defining feature of this diverse type, which consists of at least three subgroups (Taddia et al. 2013b, 2015) – slowly-evolving events such as the prototype of the class, SN 1988Z (Turatto et al. 1993), so-called type IIn-P events with a II-P-like plateau phase such as SN 1994W (Sollerman et al. 1998), and faster-declining so-called IIn-L events such as SN 1999el (di Carlo et al. 2002). Figure 3.5 illustrates the diversity of type IIn light curves (Taddia et al. 2015).

There can be multiple different, simultaneous mechanisms at work in a type IIn SN. In the early stages, the slow-moving (between 10 and a few hundred km s^{-1}) CSM is ionized by the initial flash of the SN, its recombination producing very narrow lines (e.g. Fassia et al. 2001). At this stage, the photosphere (due to scattering off electrons in the ionized medium) is in the unshocked CSM and blocks our view of the shock and the ejecta, resulting in a blue continuum with no features save the narrow Balmer series emission lines with broad Lorentzian wings from the electron scattering (Chugai 2001). Eventually the optical depth of the unshocked gas decreases and we see further in. Meanwhile, the collision between the ejecta and the CSM drives a shock wave into the CSM, also resulting in a reverse shock inward of the CSM-ejecta interface (Chevalier & Fransson 1994). The region between these shocks contains shocked, ionized CSM and produces line components with widths of a few hundred to a few thousand km s^{-1}. Radiative cooling in this region is efficient and, together with the mixing of material at the SN-CSM interface, results in the formation of a cool dense shell (CDS) (Chugai et al. 2004). Radiation and reheating from the shocks powers the continuing emission from this region. If the CSM interaction is strong enough, the photosphere may take a long time to recede to the ejecta. The CSM may very well be asymmetric (e.g. Smith et al. 2015), in which case multiple (possibly superposed) components of the Balmer lines, including those from the ejecta, can be seen simultaneously. An H α profile with multiple peaks can emerge even without asymmetry, as a result of a combination of emission from the CDS or behind it and absorption by dust formed in the CDS (Fransson et al. 2005). Radio synchrotron emission from electrons accelerated by the forward shock results in strong radio emission from CSM interaction, especially at late times (e.g. Weiler et al. 1989, 1991; Williams et al. 2002).

Type IIn SNe (of the 1988Z-like subtype) have been connected to luminous blue variables (LBVs; Humphreys & Davidson 1994), which are very

massive stars ($M_{\rm ZAMS} \gtrsim 50 M_{\odot}$) that experience strong mass loss through eruptive episodes (where the mass loss rate can temporarily reach 0.1 or even 1 $M_{\odot}$ yr^{-1}) and powerful winds (up to $10^{-3} M_{\odot}$ yr^{-1}), possibly in the process of evolving into WR stars (e.g. Gal-Yam & Leonard 2009; Smith et al. 2011b; Fransson et al. 2014). There is evidence, however, that most type IIn SN progenitors are not LBVs and are more likely to be RSGs or other lower-mass stars (Paper II; Anderson et al. 2012). The metallicities of SNe in the IIn-L subgroup point toward a similarity with type II SNe that have RSG progenitors (Taddia et al. 2015). The IIn-L group also includes objects that look like type II-L apart from the narrow lines, such as SN 1998S (Fassia et al. 2000, 2001) and SN 2008fq (Taddia et al. 2013b). For these events an RSG progenitor similar to that of a normal type II-L SN seems most likely, and the CSM could be created by a strong wind (e.g. van Dyk et al. 1999; Fassia et al. 2001). Interaction is also present in some type II-L SNe without strong narrow lines, detected e.g. through radio emission or a long-lasting blue featureless continuum (e.g. Paper III, Weiler et al. 1991), and might even be ubiquitous for type II-L (Valenti et al. 2015), blurring the line between these SN types. Some bright type II-L SNe have a tail-phase decline rate faster than expected from ^{56}Co decay – this could be due to CSM interaction powering the late phases instead (Blinnikov & Bartunov 1993), or because the γ-rays from ^{56}Co decay are not fully trapped in the ejecta (Anderson et al. 2014; Terreran et al. 2016). The progenitors of the IIn-P subgroup may be massive AGB stars exploding as electron-capture SNe (ECSNe; e.g. Kankare et al. 2012, see also Sect. 3.1.5), although Dessart et al. (2009) questioned the SN nature of the prototypical type IIn-P SN1994W, arguing that a transient with the properties of SN 1994W could be produced by the collision of ejected shells without a terminal explosion.

Another type of interacting SN is the more recently identified type Ibn. Type Ibn SNe are rare events that exhibit narrow emission lines of helium along with normal type Ib SN features, but with no or weak hydrogen emission (e.g. Shivvers et al. 2016b). The first detected extragalactic SN, SN 1885 in the Andromeda galaxy, may have been a type Ibn SN, but the prototypical event for this class was SN 2006jc (Mattila et al. 2008; Pastorello et al. 2008b). Type Ibn SNe are analogous to type IIn, but the explosion is of type Ib and the surrounding CSM consists mainly of helium. Relatively broad helium lines can also be observed in type Ibn SNe (Pastorello et al. 2016), indicating the presence of helium in the ejecta as

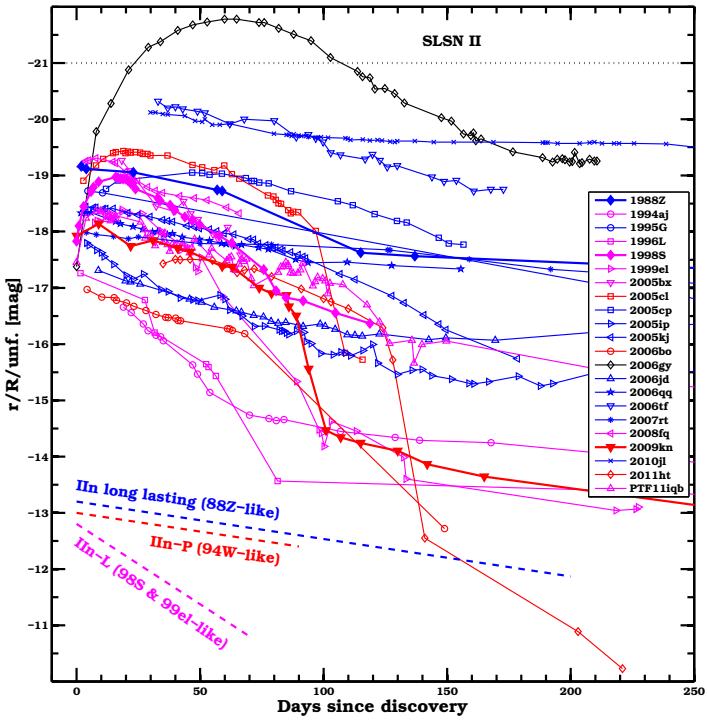

Figure 3.5: Light curves (in the r or R band or unfiltered) of a sample of type IIn SNe (Taddia et al. 2015), demonstrating the photometric diversity of this SN type, likely caused by multiple different progenitor channels.

well. Thanks to the power source provided by interaction, their luminosities tend to be higher than those of normal type Ib SNe (Pastorello et al. 2016), with some events reaching ~ -20 mag (Pastorello et al. 2015a), despite smaller explosion energies and ^{56}Ni masses possibly caused by fall-back onto a black hole (Moriya & Maeda 2016). Type Ibn SNe tend to decline faster than type IIn SNe, indicating that the interaction ceases earlier (Moriya & Maeda 2016). The type is, however, diverse, with some transitional SNe between the IIn and Ibn types (Pastorello et al. 2008c; Smith et al. 2012; Pastorello et al. 2015a) or between Ibn and Ib (Pastorello et al. 2015b). The progenitors of type Ibn SNe have been proposed to be massive WR stars (Pastorello et al. 2008b; Gorbikov et al. 2014) – where the helium-rich CSM would be produced through episodes resembling LBV eruptions – with the transitional types perhaps being LBV stars evolving toward the WR stage (Smith et al. 2012; Pastorello et al. 2015a). Two years before SN 2006jc, an LBV-like giant outburst was detected (Pastorello et al. 2007), possibly from a WR star (from which LBV-like eruptions had not been observed before) or an LBV companion. Maund et al. (2016) detected a possible binary companion to the progenitor of SN 2006jc but ruled out an LBV. The companion was instead consistent with a $\sim 10 M_{\odot}$ YSG, raising the possibility of a lower-mass binary progenitor.

Some very rare SNe show signs of interaction along with observed properties typically associated with type Ia SNe (see Sect. 3.2). Their spectra consist of multi-component hydrogen Balmer emission lines and broad absorption features of mainly hydrogen, helium, iron and calcium. These rare SNe are often called type Ia-CSM or Ia/IIn SNe (e.g. Inserra et al. 2016a; Kilpatrick et al. 2016). The prototype event is SN 2002ic (Wang et al. 2004). The nature of this SN class is under debate, with some studies favoring a type Ia SN exploding in the wind of a red giant companion (e.g. Dilday et al. 2012; Fox et al. 2015a; Kilpatrick et al. 2016) and others instead proposing a CCSN (Benetti et al. 2006; Trundle et al. 2008; Inserra et al. 2016a). More studies of this peculiar class are needed. A combination of different progenitor populations is also possible: while Inserra et al. (2016a) admitted that PTF11kx (Dilday et al. 2012) is indeed consistent with a WD progenitor like that of a type Ia SN based on its ejecta mass, they argued that SN 2012ca is best matched by a CCSN. The light curves of these events are also different, with the fainter PTF11kx exhibiting a much faster decline similar to the type Ia SN 1991T and most other type Ia-CSM SNe evolving slower (Inserra et al. 2016a).

3.1.4 Superluminous supernovae

A new class of unusual SNe has emerged in the last decade or so, with the rise of non-targeted SN surveys. Apart from some exceptions (e.g. Paper III), typical SNe do not exceed brightnesses of $M_B \sim -19.5$ mag (Richardson et al. 2014). However, SNe 2005ap (e.g. Quimby et al. 2007) and 2006gy (e.g. Ofek et al. 2007; Smith et al. 2007) were both determined to be brighter than $M \sim -22$ mag in at least one band, making them the most luminous SNe detected at the time. SNe that exceed an absolute magnitude of -21 mag in any band (making them typically tens or even hundreds of times brighter than normal SNe) are called superluminous SNe (SLSNe). The study of SLSNe is a new, fast-evolving field; SLSNe remain inadequately understood, but rapid progress has been made in the recent few years. Gal-Yam (2012) presented a review of SLSNe, dividing them into types analogously with normal CCSNe. Type I SLSNe exhibit no hydrogen features in their spectra, while type II SLSNe do. A third type, SLSN-R, was also identified – the light curves of these SLSNe were initially found consistent with being powered by large amounts of radioactive nickel. However, as these events spectroscopically resemble the faster-declining type I SLSNe (see e.g. Paper IV, Inserra et al. 2013; Nicholl et al. 2013), they are now both considered subgroups within the same class of transients. A typical early spectrum of a hydrogen-poor SLSN shows a series of O II absorption lines around 3500 – 4500 Å superimposed on a hot continuum, which typically later evolves to resemble type Ic SNe (e.g. Pastorello et al. 2010; Quimby et al. 2011). As such, this class is usually referred to as type Ic SLSNe. The class contains both the slowly-declining SN 2007bi-like events (e.g. Gal-Yam et al. 2009; Nicholl et al. 2013) and faster-evolving SN 2010gx-like events (e.g. Paper IV, Pastorello et al. 2010; Inserra et al. 2013), which may form a continuum (Paper IV, Nicholl et al. 2015). Type II SLSNe include both IIn-like events with narrow lines, such as SN 2006gy, and events with broad hydrogen lines such as SN 2008es that resemble type II-L SNe (Gezari et al. 2009; Inserra et al. 2016b). Figure 3.6 shows the typical light curves of SLSNe compared to normal SNe, while Figure 3.7 demonstrates the spectroscopic evolution of a type Ic SLSN.

SLSNe are known to be intrinsically rare, as their extreme luminosity would allow us to detect them at much larger distances than other SN types – Prajs et al. (2017) estimated the rate of SLSNe at $z \simeq 1$ to be roughly 0.02 per cent of the total CCSN rate, while the rate of type Ic SLSNe has been

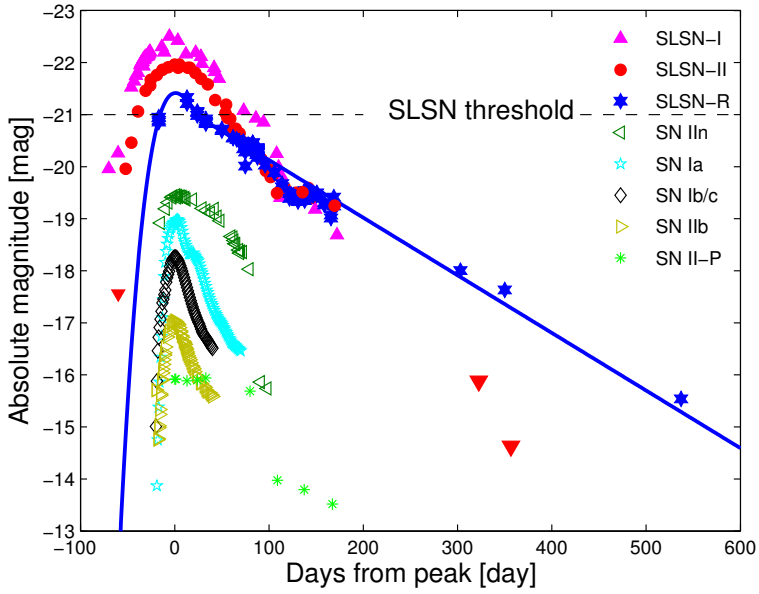

Figure 3.6: Illustrative R-band light curves of different SLSN types compared to normal SN types (Gal-Yam 2012). The SLSN-I and SLSN-R types are now often considered fast- and slowly-declining subclasses of type Ic SLSNe, respectively.

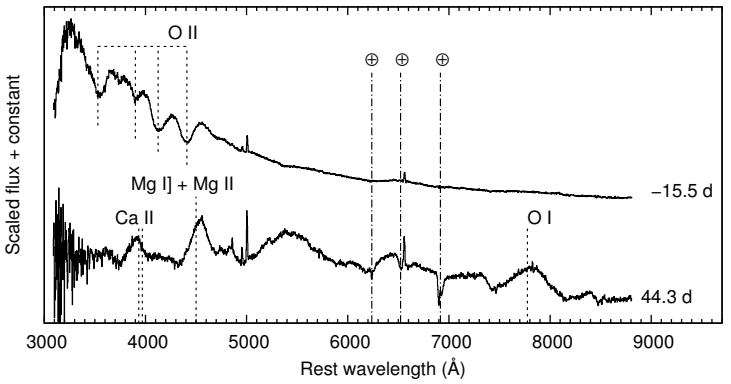

Figure 3.7: Two spectra of the type Ic SLSN Gaia16apd (Paper IV), demonstrating the typical spectroscopic evolution of this SN type. The earlier spectrum shows O II absorption lines around 3500 – 4500 Å superimposed on a hot continuum, while the later resembles a normal type Ic SN close to maximum light. Telluric absorption lines are marked with the ⊕ symbol. The narrow emission lines originate from the host galaxy.

estimated as less than 0.01 per cent by Quimby et al. (2013) and McCrum et al. (2015). Their detectability over extreme distances also makes them a candidate for a cosmological standard candle at distances unreachable using type Ia SNe (e.g. Inserra & Smartt 2014), as type Ic SLSNe exhibit an empirical relation between peak luminosity and time-scale, with brighter events also tending to evolve slower:

$$M_{400} = (1.19 \pm 0.47)\Delta M_{20} - (22.53 \pm 0.37), \tag{3.6}$$

where M_{400} is the peak absolute magnitude in a synthetic bandpass centered on 400 nm, and ΔM_{20} is the brightness decline in magnitudes over 20 days in this bandpass. The mean peak magnitude is $M_{400} = -21.64 \pm 0.46$. The number of observed SLSNe is not yet high enough to distinguish between cosmology models, however, and the physical reason for the relation remains unclear.

The host galaxies of type Ic SLSNe are typically faint and metal-poor (below 0.5 times solar metallicity) dwarf galaxies similar to the hosts of GRBs (e.g. Perley et al. 2016), with few exceptions, indicating low metal-

licity to be necessary for producing them. The hosts of the slow and fast subtypes are indistinguishable (Schulze et al. 2016). The hosts of type II SLSNe are more metal-rich and massive on average, but also more diverse in their properties (still slightly less massive than average star-forming galaxies, but this may be due to selection effects; Perley et al. 2016).

Several mechanisms have been proposed to explain the extreme energies unleashed in SLSNe. One such explanation is the so-called pair-instability SN (PISN) scenario (e.g. Barkat et al. 1967; Heger & Woosley 2002). In extremely massive stars (with ZAMS masses in excess of 140 $M_{\odot}$), after the helium-burning stage, the massive core, composed mainly of oxygen, enters a temperature and density regime where high-energy photons are converted into electron-positron pairs in large numbers. This process converts internal energy into mass, but decreases pressure, resulting in a collapse that is stopped when explosive oxygen burning begins. This runaway chain reaction completely disrupts the star, leaving behind no compact remnant. The luminosity is powered by a large amount of synthesized ^{56}Ni. However, the PISN models (by e.g. Kasen et al. 2011) have been found incompatible with recent SLSN observations (both types), where they fail to produce the observed light curve and/or spectrum (e.g. Dessart et al. 2013; Nicholl et al. 2013; Lunnan et al. 2016; Yan et al. 2016). The decay of a large mass of ^{56}Ni cannot be the primary power source, as both the required peak magnitude and the tail-phase light curve simultaneously cannot be produced self-consistently (Quimby et al. 2011).

The most popular power source for type Ic SLSNe is the magnetar spin-down scenario. A magnetar is a neutron star with a magnetic field of 10^{14} – 10^{15} gauss (G[4]). The theory of magnetars was developed by Duncan & Thompson (1992). As the star collapses into a neutron star in a SN, angular momentum and magnetic flux are conserved, drastically increasing the magnetic field and spin of a star as its radius and surface area decrease. If the spin period of the newborn neutron star is shorter than its convection time-scale (i.e. a few ms), helical motions inside it cannot be suppressed by internal turbulence and they strengthen the magnetic field through induction. Thus an efficient dynamo process takes place in the first few seconds of the existence of the neutron star, converting rotational energy into magnetic energy and boosting the magnetic field to create a magnetar. As angular momentum is efficiently lost from the core during

[4] 1 G = 10^{-4} T.

the RSG phase, the progenitors of magnetars have been suggested to be stars with ZAMS masses in excess of $\sim 25 M_\odot$ (assuming Solar metallicity) with shorter or nonexistent RSG phases (Gaensler et al. 2005). The first magnetars were discovered in the late 1990s (Kouvetouliou et al. 1998, 1999). Kasen & Bildsten (2010) found that the injection of the rotational energy of the magnetar into the SN ejecta (in the form of high-energy photons, through the decay of the magnetic field) would be enough to power a SLSN. The luminosity in a scenario where the magnetar is assumed to be the only power source (a reasonable assumption in a SLSN, which will be dominated by the magnetar output) is calculated semi-analytically as follows. The rotation period P determines the rotational energy $E_p \simeq 2 \times 10^{52}$ erg $\times$ $(P/1 \text{ ms})^{-2}$ (assuming a fixed moment of inertia $I = 10^{45}$ g cm^{-2}), while B and P together determine the spin-down time-scale $\tau_p \simeq 4.7$ d $\times (P/1 \text{ ms})^2 \times (B/10^{14} \text{ G})^{-2}$. With the assumption of uniform density, the third input parameter, the diffusion time in the ejecta τ_m, is determined by the opacity κ, ejecta mass $M_{\rm ej}$ and kinetic energy $E_{\rm k}$ as

$$\tau_m = 10\text{d} \left(\frac{M_{ej}}{1\text{M}_\odot} \right)^{3/4} \left(\frac{E_{\rm k}}{10^{51} \text{ erg}} \right)^{-1/4} \left(\frac{\kappa}{0.1 \text{ cm}^2 \text{ g}^{-1}} \right)^{1/2}. \tag{3.7}$$

Combining the Arnett (1982) light curve (Eq. 3.5) and the magnetar input by Kasen & Bildsten (2010), the luminosity evolution $L(t)$ of the SLSN, assuming it to be dominated by the magnetar power, is then described by

$$L(t) = \frac{2E_p}{\tau_p \tau_m} e^{-(\frac{t}{\tau_m})^2} \int_0^t \frac{1}{(1 + t'/\tau_p)^2} e^{(\frac{t'}{\tau_m})^2} \frac{t' dt'}{\tau_m}. \tag{3.8}$$

The integral is calculated numerically to obtain the luminosity. The peak luminosity is $L_{\rm peak} \sim \frac{E_p \tau_p}{\tau_m^2}$, which can also be expressed as

$$L_{\rm peak} \sim 5 \times 10^{43} B_{14}^{-2} \kappa_{es}^{-1} M_5^{-3/2} E_{51}^{1/2} \text{ erg s}^{-1}, \tag{3.9}$$

where B_{14} is the magnetic field in units of 10^{14} G, κ_{es} the opacity in units of 0.2 cm^2 g^{-1}, M_5 the ejecta mass in units of $5 M_\odot$ and E_{51} the explosion energy in units of 10^{51} erg.

Magnetar models similar to the one described above have been successfully employed to reproduce the light curves of type Ic SLSNe (e.g. Paper IV, Nicholl et al. 2013; Inserra et al. 2013; McCrum et al. 2014; Lunnan et

al. 2016). The magnetar model may also be responsible for the type Ic-BL SNe connected with GRBs (e.g. Wheeler et al. 2000), implying a continuum between these transient classes. The central magnetar engine blows a 'bubble' inside the SN ejecta, sweeping most of it into a thin shell (Kasen & Bildsten 2010). This results in fairly constant observed photospheric velocities as, unlike in normal SNe where the expansion is homologous and the photosphere recedes deeper into the ejecta, the photosphere remains at the shell for some time. This velocity evolution is indeed observed in type Ic SLSNe (Nicholl et al. 2015) – although this was disputed by Liu & Modjaz (2016) using a different method for measuring the velocities and taking line blending into account. Some (possibly all) type Ic SLSNe exhibit a pre-peak 'bump' in their light curve, which can be explained by the magnetar model as the breakout of a shock driven by the formation of the central bubble (e.g. Nicholl & Smartt 2016) – however, more detailed simulations are needed. The ejecta masses of type Ic SLSNe (of both subtypes) seem to be consistent with single WR stars exploding in what would be a normal type Ic SN, but combined with the magnetar input (e.g. Paper IV, Nicholl et al. 2015; Jerkstrand et al. 2016b), which is consistent with Gaensler et al. (2005) if the progenitor mass is determined to be above $\sim 35 M_{\odot}$. Signs of the presence of a massive binary companion have also been found in the ejecta of a type Ic SLSN, however (Moriya et al. 2015), in which case the early bump in the light curve could be explained by the collision between the ejecta and the companion star.

Another plausible power source is interaction with a CSM, analogous to the process in normal type IIn SNe. For type Ic SLSNe, CSM interaction requires some fine-tuning in the mass and structure of the CSM to produce the light curve (Nicholl et al. 2015), and furthermore, no signatures of interaction are visible in the spectra of type Ic SLSNe (Nicholl et al. 2014). For type IIn SLSNe, interaction is a natural explanation: SN 2006gy and its evolution over several years can be explained with a $\sim 10 M_{\odot}$ dusty shell of CSM (Fox et al. 2015b). A possible way to produce a massive CSM is pulsational pair instability, a process where pair production creates an instability that does not lead to a PISN explosion but a non-terminal eruption (Heger & Woosley 2002; Woosley et al. 2007). Tolstov et al. (2016) used the CSM interaction model, with the CSM originating from pulsational pair-instability, combined with ^{56}Ni decay, to reproduce the light curve of PTF12dam. Eruptions in an LBV can also cause this kind of mass loss. In any case, a very massive star is required to create a type IIn SLSN.

The other, smaller group inside type II SLSNe, the II-L-like events with broad hydrogen lines, may be explained by magnetar powering and/or CSM interaction (although the velocity evolution of SN 2008es disfavors the CSM scenario; Gal-Yam 2012), possibly a combination of both (Inserra et al. 2016b). Whatever the mechanism powering the light curve, it seems that the progenitor star has retained a significant hydrogen envelope (Gal-Yam 2012). More work is needed to understand this small subclass of SLSNe.

A class of transients called tidal disruption events (TDEs) has been recently discovered (Gezari et al. 2003). In a TDE, a star is disrupted by tidal forces as it approaches a black hole of sufficient mass and approximately half of the star is ejected (assuming Newtonian tidal forces), while the rest is accreted by the black hole (Rees 1988). These events are outside the scope of this thesis, but it is worth mentioning that they can exhibit SLSN-like light curves and temperatures (e.g. Arcavi et al. 2014), and a classification of a transient at the nucleus of its host galaxy as a SLSN or a TDE can be ambiguous. SN 2015L (commonly called ASASSN-15lh), initially considered the brightest SN ever discovered (Dong et al. 2016), is more likely to have been a TDE, where a spinning supermassive black hole disrupted a star (Leloudas et al. 2016).

3.1.5 Electron-capture supernovae

The minimum ZAMS mass for the progenitor of a normal CCSN seems to be around 8 or 9 $M_\odot$ (e.g. Smartt 2009). Below this limit, nuclear fusion does not continue past magnesium and the electron-degenerate core of the star in its final stages consists of oxygen, neon and magnesium. A core such as this can, however, also explode through a different mechanism. As the core grows, its density increases until a critical value of $\sim 4 \times 10^9$ g cm^{-3} is reached; at this point the protons in magnesium nuclei begin to capture electrons from the core, the electron degeneracy pressure suddenly decreases and the core collapses (e.g. Miyaji et al. 1980; Nomoto 1984, 1987; Tominaga et al. 2013). As in normal CCSNe, this collapse is followed by a bounce and shock breakout, resulting in the explosion of the star in an electron-capture SN (ECSN). The explosion energy of an ECSN would be on the order of 10^{50} erg. However, Jones et al. (2016) argued that the collapse may trigger a thermonuclear explosion of the oxygen and eject a part of the core, leaving behind a WD instead of a neutron star.

Stars in the phases immediately before an ECSN are massive AGB

stars, also called super-AGB (sAGB) stars, in a narrow ZAMS mass range of roughly 7 – 8 $M_\odot$ (assuming solar metallicity and convective overshoot in the core; Siess 2007). Such stars still retain a massive hydrogen envelope, and SNe from sAGB progenitors are expected to be of type II (Nomoto 1987). Strong mass loss is also present in sAGB stars, and some type IIn SNe have been associated with ECSNe, e.g. the subluminous SN 2008S (Botticella et al. 2009) and the subclass of type IIn-P SNe (e.g. Kankare et al. 2012). Simulations by Moriya et al. (2014) support the association between type IIn-P SNe and ECSNe from sAGB progenitors; the plateau in the light curve would be analogous to normal type II-P SNe. In addition, SN 1054, which produced the Crab Nebula, may have been an ECSN (Smith 2013; Moriya et al. 2014). Because of the large fraction of binary systems among O- and B-type stars, Moriya & Eldridge (2016) also investigated the possibility of stripped-envelope ECSNe and found them to possibly be related to faint, peculiar so-called type Iax SNe. However, despite the aforementioned candidates, the existence of ECSNe is still uncertain.

3.2 Thermonuclear supernovae

Type Ia SNe are defined by a lack of hydrogen or helium signatures in their spectra and the presence of broad absorption features of several metals, mainly silicon (especially Si II at 6155 Å), iron and calcium, around the time of maximum light (Filippenko 1997). They constitute roughly a quarter of all SNe in a volume-limited sample (Li et al. 2011a). They are, on average, nearly 2 mag brighter than CCSNe other than type IIn ($\langle M_{B,\mathrm{Ia}}\rangle = -19.3 \pm 0.2$ compared to $\langle M_{B,\mathrm{II-P}}\rangle = -16.8 \pm 0.4$ or $\langle M_{B,\mathrm{Ic}}\rangle = -17.7 \pm 0.4$, for example; Richardson et al. 2014), and as such they are detected at a larger distance, resulting in a fraction of almost half of all known SNe. Figure 3.8 demonstrates a typical photospheric-phase spectrum of a type Ia SN.

Hoyle & Fowler (1960) suggested, based on the chemical compositions of type Ia SNe and their remnants, and the energy budgets of the explosions, that the origin of such a SN is the thermonuclear burning of an electron-degenerate stellar core. Type Ia SNe, unlike CCSNe, are not preferentially located in young stellar populations (van Dyk 1992), which points toward progenitor stars much older and thus less massive than those of CCSNe. The lack of light elements in these events, in addition to the ages of the

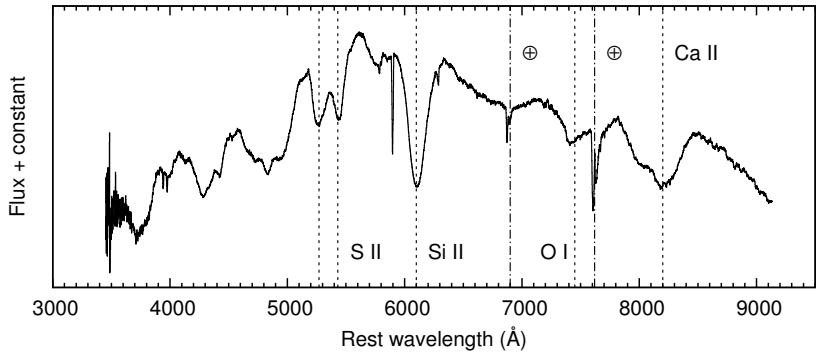

Figure 3.8: Spectrum of a normal well-studied type Ia event, SN 2014J, near maximum light with some prominent spectral lines identified (Srivastav et al. 2016). Telluric absorption lines are marked with the ⊕ symbol.

stellar populations, points toward carbon-oxygen WD progenitors. This is indeed the present established picture of type Ia SN progenitors: a WD accreting matter until its mass is $\sim 1.4 M_\odot$ (depending on rotation), close to the Chandrasekhar limit but not quite reaching it (e.g. Maoz et al. 2014). At this point the temperature in the core of the WD is high enough to start carbon fusion (Nomoto 1982). The degenerate matter of the WD then undergoes an unstable runaway thermonuclear reaction that completely unbinds the star and fuses $\sim 0.6 M_\odot$ of the carbon and oxygen into ^{56}Ni. The details of this chain reaction are not completely understood, but one leading scenario is that the fusion begins as a front propagating at subsonic velocities (*deflagration*), perhaps starting slightly away from the center of the WD, before somehow turning into a supersonic shock wave (*detonation*). This is the so-called delayed detonation model introduced by Khokhlov (1991). As with type Ib/c SNe, the radioactive decay of ^{56}Ni into ^{56}Co and then ^{56}Fe powers the characteristic light curve. A secondary red peak is caused by absorption of blue wavelengths in Fe II ions, and re-emission in the near-infrared (NIR), when the temperature declines and the recombination of Fe III to Fe II increases (Kasen 2006). The uniform progenitors of type Ia explosions result in their usefulness as cosmic distance indicators (but see below for caveats); although the luminosities of different type Ia SNe are not identical, a tight empirical relation exists between the peak absolute

magnitude of the SN and the decline rate of the B-band light curve (Phillips 1993):

$$M_{\max,B} = (-21.726 \pm 0.498) + (2.698 \pm 0.359)\delta m_{15}(B) \text{ mag}, \qquad (3.10)$$

where $\delta m_{15}(B)$ is the decline in B-band magnitude in the first 15 days after the peak. This relation has made it possible to use type Ia SNe to measure cosmological distances relatively precisely and to thus infer the acceleration of the expansion of the universe (Riess et al. 1999; Perlmutter et al. 1999).

The WD can accrete matter either from a companion star such as a red giant (the single-degenerate or SD scenario Whelan & Iben 1973), or by merging with another WD in a tight binary after having lost angular momentum through gravitational waves (the double-degenerate or DD scenario Iben & Tutukov 1984), and the uncertainty of which channel is dominant is called the 'SN Ia progenitor problem' (Maoz & Mannucci 2011). Too much fine tuning may be required in the SD scenario to keep the mass accretion in a range where the WD does not grow into a red giant (e.g. Maoz et al. 2014); however, the DD scenario is not without its own problems. Collisional DD events should be rare, while less violent mergers (whose numbers could be sufficient) may result in a collapse to a neutron star instead. The SD scenario was long considered the dominant channel, but the tide has been turning against it in recent times. Recent observations of nearby type Ia SNe 2011fe and 2014J favor the DD scenario at least for these particular events, as no material from the non-degenerate companion has been detected (Pérez-Torres et al. 2014; Lundqvist et al. 2015), nor can a red giant companion be found in pre-explosion images of the location of either SN (Li et al. 2011b; Kelly et al. 2014). Conversely, as Maoz et al. (2014) conclude, currently DD progenitors cannot be ruled out, and the DD channel may turn out to be dominant. This would make type Ia SNe problematic as distance indicators since the total mass of the two WDs is not necessarily close to the Chandrasekhar limit. The progenitor problem is still not sufficiently resolved, however.

Models for sub- or super-Chandrasekhar type Ia SNe also exist. A so-called double-detonation scenario involves the slow transfer of helium from a non-degenerate or helium WD companion, resulting in an explosive helium ignition that then causes a carbon ignition even in a sub-Chandrasekhar-mass WD (Livne 1990). Some observations, on the other hand, suggest a super-Chandrasekhar-mass progenitor based on the ejected mass of ^{56}Ni

(e.g. Howell et al. 2006). If the WD rotates fast enough, it may be able to support a super-Chandrasekhar mass without igniting. Explosions of such nonstandard progenitors would not comform to the brightness-decline relation of normal type Ia SNe and thus could contaminate cosmological distance measurements that use type Ia SNe. Multiple kinds of peculiar type Ia SNe, such as the low-luminosity, so called type Iax (e.g. Foley et al. 2013), the overluminous SN 1991T-like SNe (e.g. Filippenko et al. 1992) and the spectroscopically peculiar SN 1991bg-like SNe (Leibundgut et al. 1993), have been observed, which further complicate the thermonuclear SN picture but are outside the focus of this thesis.

3.3 Supernova impostors

Some SN-like transients are instead non-terminal outbursts of massive stars similar to the Great Eruption of η Carinae in the 19th century. These events were named 'SN impostors' by van Dyk et al. (2000), as they are sometimes mistaken for type IIn SNe and discovered serendipitously by SN searches. However, SN impostors are fainter than true SNe, reaching absolute magnitudes roughly from -10 to -15 mag, and their spectra lack the signatures of metals synthesized in CCSNe (e.g. van Dyk et al. 2000; Maund et al. 2006; Tartaglia et al. 2015; Kankare et al. 2015; Tartaglia et al. 2016a,b). Taddia et al. (2015) found lower metallicities for impostors than for type IIn SNe. Like the eruption of η Carinae, they have been connected to the giant eruptions of LBVs. An impostor event sometimes immediately precedes a true type IIn (or Ibn) SN (e.g. Pastorello et al. 2007; Smith et al. 2014; Tartaglia et al. 2016b), and such eruptions may be responsible for the ejection of the CSM that the SN ejecta interacts with. A particularly controversial event, SN 2009ip, may have been a SN preceded by an impostor (e.g. Smith et al. 2014), or it may instead have been caused by two colliding shells ejected in SN impostor eruptions (e.g. Pastorello et al. 2013) – neither has been conclusively disproven (Fraser et al. 2015). Dessart et al. (2009) suggested the colliding shell scenario instead of a true SN for SN 1994W as well. In addition to LBVs, lower-mass stars such as RSGs or BSGs could cause SN impostor eruptions (e.g. Smith et al. 2015). Kankare et al. (2015) suggested a yellow hypergiant (YHG) progenitor for one SN impostor, and Tartaglia et al. (2016a) found another consistent with a YSG with a mass of 18 – 20 $M_{\odot}$.

The mechanism for the eruptive mass loss is uncertain. Luminosities near the Eddington limit (beyond which the gravity of the star cannot resist the radiation pressure from inside the star), caused by a sudden unexplained increase in the luminosity of the star (e.g. Humphreys & Davidson 1994), have long been considered the immediate cause, but the eruptions of non-LBV stars, which should never approach the Eddington limit, have cast doubt on this view (Smith 2014). The diversity, type IIn SN-like spectra and high ejecta velocities of SN impostors (Smith et al. 2011c) suggest hydrodynamic explosions and subsequent interaction between a shock and CSM – or possibly eruptions caused by binary interaction – instead of super-Eddington winds (Smith 2014). In both cases the trigger of the sudden brightening or the shock remains unexplained, and in case of the CSM interaction the CSM would have to be ejected through winds or prior eruptions. Pulsational pair instability eruptions would also create SN impostors (e.g. Heger & Woosley 2002).

3.4 Failed supernovae

It has been suggested that some massive stars fail to explode as a CCSN (e.g. Woosley 1993; Fryer 1999; O'Connor & Ott 2011). In this case the energy deposition from neutrinos (or other power source) that would normally revive the stalled shock is too weak to do so, and fall-back onto the formed neutron star causes it to collapse into a black hole. Fryer (1999) found that stars in their simulations collapsed into black holes above ZAMS masses of $\sim 25 M_\odot$, and failed to produce a SN above $40 M_\odot$. Horiuchi et al. (2014) found that a core compactness parameter

$$\xi_{2.5} = \frac{M/M_\odot}{R(M = 2.5 M_\odot)/1000\mathrm{km}}, \tag{3.11}$$

where $R(M = 2.5 M_\odot)$ is the radius containing a mass of $2.5 M_\odot$, determines whether the star is able to explode. A compactness of $\xi_{2.5} \gtrsim 0.2$ was found to lead to a failed SN. As a solution to the problem of missing high-mass RSG progenitors of type II SNe, Horiuchi et al. (2014) and Smartt (2015) suggested that stars above ZAMS masses of $\sim 16.5 M_\odot$ or $\sim 18 M_\odot$, respectively (and depending on metallicity), would collapse directly into black holes, apart from islands of explodability caused by the complex relationship between mass, metallicity and core compactness. Different theoretical

studies disagree on where these islands should lie (e.g. Heger et al. 2003; Pejcha & Thompson 2015; Ertl et al. 2016). As an example, Ertl et al. (2016) predict explodability at several initial masses around $20M_{\odot}$, in the 25 – 27 $M_{\odot}$ range and at 60, 80, 100 and 120 $M_{\odot}$ at Solar metallicity.

From our perspective, the progenitor of a failed SN would simply seem to disappear (or perhaps produce a faint transient and/or a GRB; Woosley 1993; Lovegrove & Woosley 2013). A pre-collapse eruption observable as a SN impostor is also a possibility (e.g. Smith et al. 2011c). Reynolds et al. (2015) searched for vanished massive stars in *Hubble Space Telescope* (*HST*) archival data, checking if stars were visible when images of galaxies with multiple epochs of observations were subtracted from each other. With a distance limit of 28 Mpc, 15 galaxies were included and one plausible candidate for a failed SN was found. Another survey using the Large Binocular Telescope (Adams et al. 2016a,b), which included data of 27 galaxies within 10 Mpc over a period of seven years, also produced one candidate. The subject of failed SNe remains debated, however, and more definitive detections are needed to confirm their existence.

Chapter 4

Supernova progenitor studies

4.1 Direct progenitor detection

The most straightforward way to study the progenitors of CCSNe is to find deep, high-resolution pre-explosion images of the explosion site, such as images from the *HST*. If the spatial resolution is good enough, a source corresponding to the precise location of the SN can be detected and placed on a Hertzsprung-Russell diagram. Later on, when the SN has faded below the brightness of this source, its disappearance may be confirmed and it can be firmly connected to the SN progenitor. Endpoints of stellar evolution models can then be compared to the progenitor to constrain its mass and spectral class. An example of such a progenitor detection is presented in Figure 4.1, and comparisons to stellar evolution tracks are presented in Figure 4.2. Recent reviews by Smartt (2009, 2015) detail the results of such progenitor searches.

Currently, no direct detections of type Ic SN progenitors exist, possibly because of their faintness in the optical bands (Yoon et al. 2012) – most of the radiation from such hot stars would be in the UV instead. One type Ib SN progenitor, that of iPTF13bvn, has been detected (Cao et al. 2013). The disappearance of the progenitor was confirmed by Folatelli et al. (2016), and it was constrained to be a 10 – 12 $M_{\odot}$ star in a binary system (Eldridge & Maund 2016) instead of a more massive WR star. In addition, a few type IIb SN progenitors have been detected (e.g. Aldering et al. 1994; Maund et al. 2004; van Dyk et al. 2011; Folatelli et al. 2014; Fox et al. 2014; Maeda et al. 2014; Folatelli et al. 2015; Tartaglia et al. 2016c). They tend to be consistent with interacting binary YSGs or BSGs (although the proposed binary companion of the SN 2011dh progenitor was disputed by Maund et al. 2015a) with ZAMS masses in the 13 – 19 $M_{\odot}$

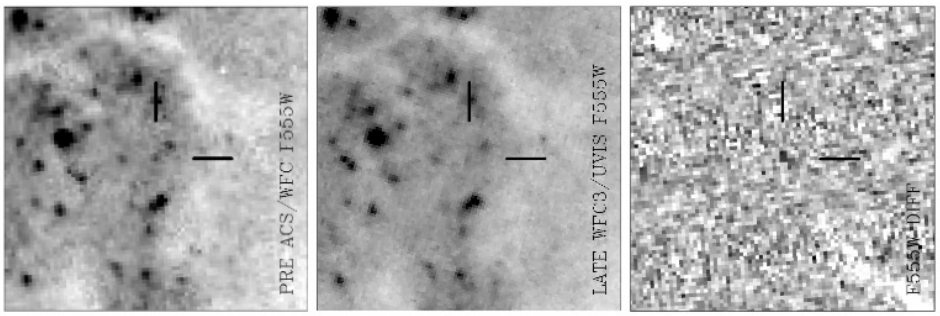

Figure 4.1: *HST* pre-explosion (left panel) and post-explosion (middle panel) images of the site of the type Ib SN iPTF13bvn, and a subtraction between the two (right panel). The images show the progenitor star and its disappearance (Eldridge & Maund 2016).

range (van Dyk et al. 2011; Maund et al. 2011; van Dyk et al. 2014; Folatelli et al. 2015). A WR progenitor was ruled out for SN 2008ax (Folatelli et al. 2015). Maeda et al. (2015) found that the more extended progenitors may still be undergoing binary interaction, while for the less extended ones this phase would be over. A few type IIn events have been connected to an LBV progenitor (e.g. Gal-Yam & Leonard 2009; Smith et al. 2011b; Fransson et al. 2014), along with events such as SN 2009ip and SN 1961V where the disappearance of the progenitor has not yet been firmly ascertained (e.g. van Dyk & Matheson 2012; Fraser et al. 2015). The (probably) only detected progenitor of a type II-L SN, that of SN 2009hd, was likely a high-mass RSG (Elias-Rosa et al. 2011).

Thus most of the directly detected SN progenitors so far are those of type II-P SNe (Smartt 2015), yielding a well established progenitor scenario for this type. Well-constrained examples include SN 2008bk (Mattila et al. 2008; Maund et al. 2014), whose progenitor was determined to be a highly reddened RSG with $M_{\mathrm{ZAMS}} = 12.9^{+1.6}_{-1.8} M_{\odot}$, and SN 2012aw (Fraser et al. 2012; Fraser 2016) with another initially $12.5 \pm 1.5 M_{\odot}$ RSG progenitor. 26 progenitors with either determined mass ranges or upper mass limits are reported in Smartt (2015), who used these masses to infer RSGs in a mass range of $9.5^{+0.5}_{-2} M_{\odot}$ to $16.5 \pm 2.5 M_{\odot}$ to be the type II-P progenitors, in reasonable agreement with earlier estimates (e.g. Smartt 2009).

The peculiar type II SN 1987A is an extremely well-studied case. The

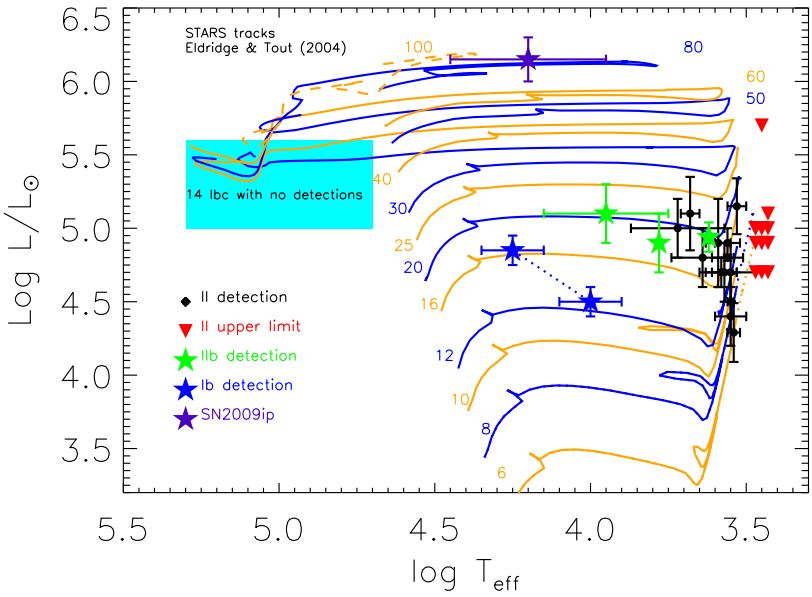

Figure 4.2: Effective temperatures and luminosities of detected SN progenitors in the HRD, compared to STARS single-star evolution models by Eldridge & Tout (2004) from Smartt (2015), showing the cluster of type II SN progenitors in the 8 – 16 $M_{\odot}$ ZAMS mass range and the lack of other progenitor detections. The lines correspond to evolutionary tracks and are labeled with ZAMS masses. The endpoints of the tracks correspond to where a star should be at the time of its death.

closest SN discovered since the 17th century (excluding SN remnants), it exploded in the LMC, only 50 kpc away (e.g. Woosley et al. 1987), close enough that its progenitor could be precisely pinpointed to be the BSG Sk -69° 202 (e.g. Walborn et al. 1987). The $20M_{\odot}$ progenitor was later suggested to have been the result of a merger of two stars with masses of 5 and $15M_{\odot}$ (Morris & Podsiadlowski 2009), which would also produce the distinctive triple-ring pattern of CSM in the SNR.

Despite the demonstrated effectiveness of the direct detection method, there are some caveats. Because of the optical faintness of type Ic SN progenitors, whether they are WR stars or not (Yoon et al. 2012; Groh et al. 2013b), detecting them is currently very difficult. As very few progenitors of SNe other than types II-P and IIb have been detected (e.g. Smartt 2015), studying types II-L and Ib, not to mention peculiar subclasses, is also difficult using this method. In addition, a very good spatial resolution is required to resolve the individual progenitor stars (in both the pre- and post-explosion images), necessitating the use of a space telescope such as *HST* or ground-based adaptive optics facilities, the observing time for which is in short supply. Even with these telescopes, only the progenitors of relatively nearby SNe can be studied, sometimes only in one or a few bands, and the stars themselves are in a relatively poorly understood phase of their evolution and possibly variable, resulting in uncertainties in the models. The extinction toward the SN may be lower than toward the progenitor as well, as the explosion evaporates dust around it, causing more uncertainty. These limitations make it necessary to seek other ways of studying SN progenitors.

4.2 Environmental studies

In addition to directly detecting progenitors in pre-explosion images, indirect methods can be employed to study the progenitors through various indicators in their environments. The advantages of indirect methods are that pre-explosion images of the SNe do not need to exist, and that the requirements for spatial resolution can be much less stringent, allowing the inclusion of more distant SNe. Therefore large samples of SNe can be studied statistically. Types without progenitor detections, such as type Ic, can also be studied in these ways. Some of these methods, and results obtained using them, are detailed below.

4.2.1 The NCR method

The basis for using the H α emission of SN host galaxies to study the masses of the progenitors is, at first glance, simple. Young, massive stars (mostly of spectral type B1 and earlier) create UV radiation energetic enough to ionize the hydrogen in the surrounding ISM, the recombination of which produces emission in the Balmer series, most predominantly the H α line[1]. H α emission thus traces star formation on timescales of $\lesssim 20$ Myr, corresponding to $M_{\mathrm{ZAMS}} \gtrsim 10 M_{\odot}$ (Kennicutt 1998). Large star-forming complexes can host multiple generations of stars, making their life-times potentially several tens of Myr (Crowther 2013). CCSNe originate in stars with $M_{\mathrm{ZAMS}} \gtrsim 8 M_{\odot}$, with lifespans $\lesssim 38$ Myr according to the Geneva group stellar evolution tracks assuming Solar metallicity (Ekström et al. 2012). Many of these stars are massive enough to produce their own region of ionized ISM, called an H II region, and some of the rest are born in large complexes with multiple stars and longer H α emission time scales. Therefore there is a clear qualitative connection between CCSNe, massive stars and H α emission.

James & Anderson (2006), hereafter JA06, developed the pixel statistics method that makes use of this connection to statistically constrain the masses of CCSN progenitors. They asserted that, as a CCSN progenitor star evolves, its native H II region, created by it and other massive stars around it, gradually dissipates as the stars in it eventually die, and the star itself may drift out of it over its lifespan. Therefore, the H α emission around the star will gradually diminish before it explodes as a CCSN. However, the more massive the progenitor, the less time there is for the H II region to dissipate, as well as for the star itself to move[2]. Therefore, only the most massive stars should still accurately trace the H α emission at the times of their explosions. To investigate the masses of the progenitors of different types of CCSNe, JA06 introduced the *normalized cumulative rank pixel value function*, or NCRPVF, which was shortened to NCR in later papers (e.g. Anderson et al. 2012, hereafter A12). A very similar method was used slightly earlier to study GRB host galaxies in the B band by Fruchter et al. (2006), who found long GRBs to correspond to the brightest spots in

[1] This line originates from the transition of the electron in the hydrogen atom from the $n = 3$ energy level to $n = 2$. Most of the emission from the $n = 2 \rightarrow n = 1$ transition is absorbed through the reionization of the hydrogen.

[2] As previously mentioned, the lifespan of a $8 M_{\odot}$ star is 38 Myr; on the other hand, a $20 M_{\odot}$ star only lives for 8 Myr and a $50 M_{\odot}$ star for 4 Myr (Ekström et al. 2012).

their host galaxies and thus to extremely massive stars.

Assume that the pixels of a continuum-subtracted H α emission map of the CCSN host galaxy are ranked from faintest to brightest in an ascending sequence. The definition of NCR, explicitly formulated in Paper I, is then

$$\mathrm{NCR}_n = \sum_{i=1}^{n} P_i / \sum_{j=1}^{m} P_j \qquad \text{, when} \sum_{i=1}^{n} P_i > 0 \tag{4.1}$$

$$\mathrm{NCR}_n = 0 \qquad \text{, when} \sum_{i=1}^{n} P_i \leq 0. \tag{4.2}$$

Here n is the rank of a pixel, NCR_n the NCR value of this pixel, P_i the flux in a pixel with rank i, and m the total number of pixels in the image. Thus each pixel in the image is assigned a value running from 0 ('background'; no H α emission) to 1 (the brightest pixel of the galaxy). Assuming that the sky background and the continuum emission of the galaxy have been properly subtracted, the average value of pixels outside the H α-emitting regions of the host galaxy is zero, with not necessarily an equal number of positive and negative pixels, but with an equal amount of positive and negative flux (i.e. counts); in this case there is no difference between different image sizes as long as all of the galaxy emission is included. When the pixels are arranged in a sequence of ascending value, the sum of all pixels at the rank corresponding to the faintest H α-emitting region (pixel) of the galaxy is the sum of the values of all pixels with no H α emission (the background pixels) and thus zero. All pixels below this rank are thus assumed to be background pixels and are assigned an NCR of zero. An example of an H α map used in an NCR calculation is shown in Figure 4.3, and an illustrative example of this is presented in Figure 4.4.

An object whose location is known can be pinpointed to a pixel in its host galaxy and assigned an NCR value. From the definition of NCR, it follows that *the NCR value of a pixel measures the fraction of the galaxy flux that originates in fainter pixels.* Therefore, if a population of objects, such as a hypothetical population of CCSN progenitors of a certain mass range, perfectly traces the H α emission, the distribution of their assigned NCRs is uniform between 0 and 1 and has an average value of exactly 0.5. Thus, for example, 60 per cent of these hypothetical objects are located in pixels containing 60 per cent of the host H α emission, and have NCR values lower than 0.6.

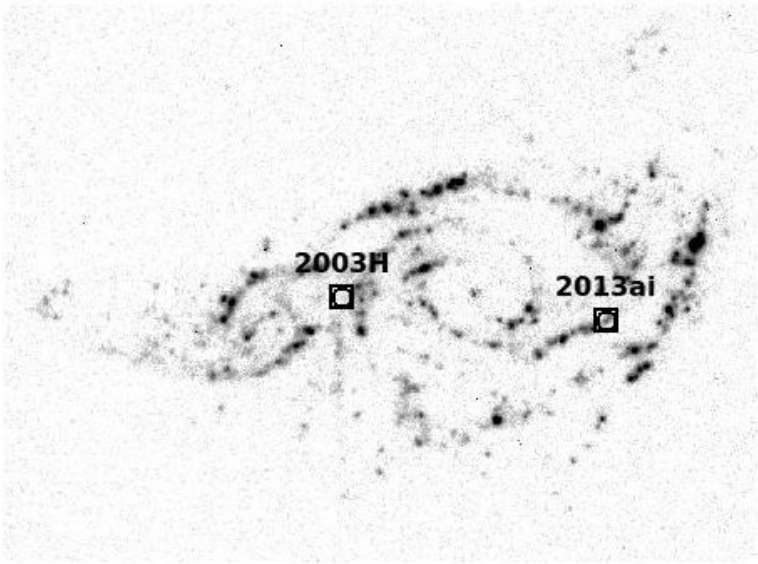

Figure 4.3: An example H α image of a galaxy pair (NGC 2207 and IC 2163, at a distance of $\sim$ 25 Mpc), observed with the Nordic Optical Telescope (NOT), to be used in an NCR calculation. The locations of two SNe hosted by the system are marked. The angular size of the system in H α is roughly 5 arcmin. In this case, SN 2003H is located in an area with relatively weak H α emission, and has NCR = 0.364, while SN 2013ai, at a more strongly star-forming region, has NCR = 0.790.

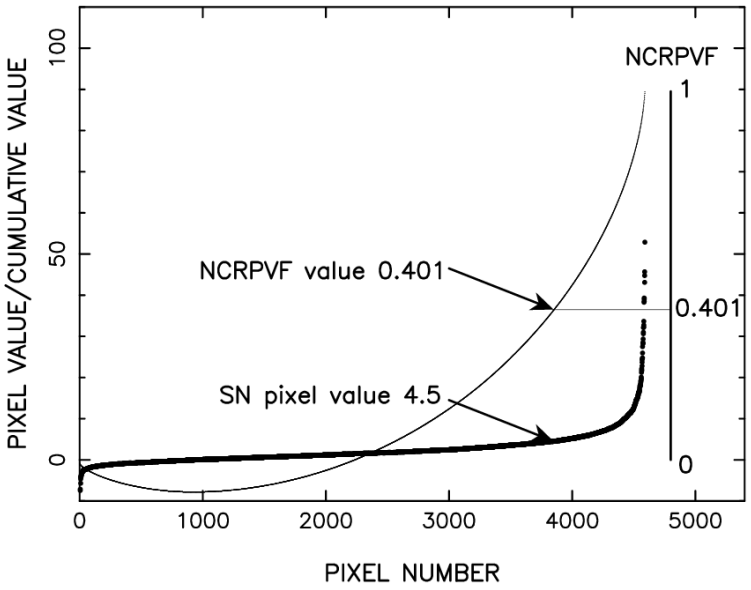

Figure 4.4: Illustrative image of how the NCR of a pixel is calculated. The ascending sequence of individual pixel values is plotted in dots, while the sum of all pixel values up to the corresponding pixel number, normalized by dividing by the sum of all pixel values, is represented by the thin line. The zero-point of the thin line corresponds to the rank where the background pixels end and the H α-emitting galaxy pixels begin. In this example, a pixel containing a SN has a number (i.e. rank) close to 4000; the value of the pixel is 4.5; and the corresponding NCR value, obtained by dividing the sum of all pixel values up to this rank by the sum of all pixel values in the image, is 0.401.

In practice, however, the background and continuum subtractions are not perfect, resulting in some background pixels with nonzero NCRs and/or galaxy pixels with zero NCRs. Additionally, the locations of SNe and other objects may have uncertainties which affect their assigned NCRs. There are some caveats in the basis of the method as well: projection effects, especially in galaxies that are inclined with respect to the line of sight, can result in a SN being apparently located in an unrelated bright H II region; multiple 'generations' of stars can be hosted by the same large H II complex (Crowther 2013), resulting in stars with low masses but high NCRs; conversely, a high-mass star can be located in a small H II region and have a low NCR; a long-lived star may drift from its native H II region into another; and the star-formation histories of different galaxies may have an effect on which mass corresponds to which mean NCR. In addition, some systematic effects are caused by the quality of the image (high noise decreases low NCRs, while low spatial resolution increases them) and the distance of the galaxy (large distances increase low NCRs) – see A12 and Papers I and II for more details. However, as the *likelihood* of a star having a high NCR is still dependent on its ZAMS mass, the method can be used to constrain CCSN progenitor masses when applied statistically to large samples of SNe. Distributions of NCR values can be compared to each other using statistical tests such as the Kolmogorov-Smirnov (KS) test and using mean NCRs.

Apart from my own work, described in Papers I and II and in Chapter 5, the NCR method has been used in several papers since its introduction. JA06 applied the method to a sample of 63 SNe (12 type Ia, 8 Ib/c, 30 type II and 13 unclassified) in 50 galaxies with recession velocities of ≤ 3000 km s^{-1}. Using this sample, they found a sequence of rising NCR (and thus presumably rising progenitor mass) with SN type: Ia $\rightarrow$ II $\rightarrow$ Ib/c. Types Ia and II were found to have a low degree of association with recent star formation, while type Ib/c SNe were found consistent with the underlying H α emission of their host galaxies, with a mean NCR of 0.490 ± 0.121 (where the uncertainty is the standard error of the mean), close to 0.5. The sample was increased for the following study by (Anderson & James 2008), who found a similar result, with the addition that type II-P SNe were found consistent with a large fraction of their progenitors having $M_{\mathrm{ZAMS}} \leq 10 M_{\odot}$. A12 continued this work further, also applying the NCR method to the near-ultraviolet (NUV) emission of the SN host galaxies. NUV emission traces star formation at a longer time scale of $\sim$ 100 Myr, since stars

not massive and blue enough to create H II regions (i.e. with a spectral class roughly B2 or later and $M_{\rm ZAMS} \lesssim 10 M_{\odot}$) can still emit in the NUV (Gogarten et al. 2009). The A12 sample of SNe was the largest, and the results thus most reliable, in an NCR study to date, with 260 CCSNe in host galaxies with recession velocities of ≤ 10000 km s^{-1} (median recession velocity 1874 km s^{-1}) – 58 of type II-P, 13 II-L, 48 simply classified as type II, 19 IIn, 13.5 IIb (one had an uncertain Ib/IIb classification), 39.5 Ib, 52 Ic and 5 Ib/c. In addition, they included 98 type Ia SNe for comparison. Their main results were as follows (the results from H α images are presented in Figure 4.5):

- in H α, type Ic SNe were found consistent with the host galaxy emission (and thus recent star formation) with a mean NCR of 0.469 $\pm$ 0.040, establishing their progenitors as the most massive;
- types Ib and II-P were found to show a significantly lower correlation (mean NCR 0.318 $\pm$ 0.045 for type Ib and 0.264 $\pm$ 0.039 for type II-P) with H α emission, and consistent with each other within 2 σ, indicating that both types had progenitors with lower mass than those of type Ic;
- in the NUV, type II-P SNe were found consistent with the host galaxy emission and thus with older star formation, supporting the H α results;
- type IIn SNe, surprisingly, had the lowest NCR values of all CCSNe, contrary to the popular claims that their progenitors are massive stars such as LBVs.

The A12 results were corroborated by Galbany et al. (2014), who had a smaller sample but applied a number of methods (see below), and by Paper I which concentrated on CCSNe in strongly star-forming galaxies specifically. In Paper II, the NCR distributions of stars in nearby galaxies were compared to those of SNe, and both type Ib and II-P SNe were found consistent with progenitor ZAMS masses $\gtrsim 9 M_{\odot}$, while type Ic SNe were consistent with ZAMS masses $\gtrsim 20 M_{\odot}$. The NCR method was also employed by Habergham et al. (2014) to study type IIn SNe and SN impostors in more detail than A12, but with similar results. Type IIn SNe were confirmed to have the lowest NCR of all CCSNe (mean NCR 0.225 $\pm$ 0.058), while the NCRs of SN impostors were even lower (although still

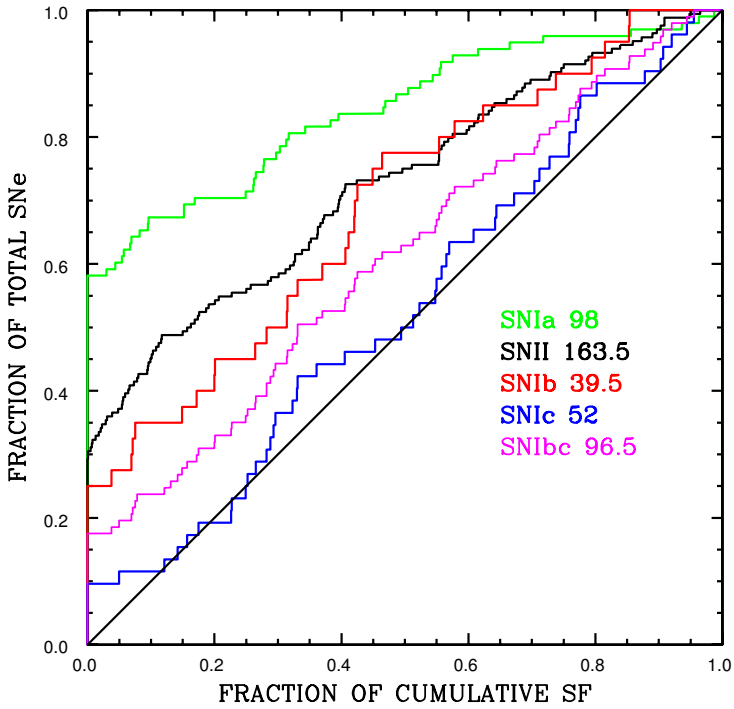

Figure 4.5: Cumulative NCR distributions of different types of SNe from A12, demonstrating the trend of increasing NCR (and thus progenitor mass) from type Ia through II and Ib to Ic. A distribution with higher NCR values is located toward the bottom right of the figure, while the diagonal line corresponds to a population perfectly tracing the underlying H α emission of the host galaxy.

consistent within 2 σ; mean NCR 0.133 $\pm$ 0.082). The conclusions were that the progenitor systems of both classes of transient are most likely diverse instead of predominantly being very massive ($M_{\mathrm{ZAMS}} \gtrsim 50 M_{\odot}$) LBV stars. Additionally, Anderson et al. (2015) used the method to analyze the environments of 102 type Ia SNe in H α as well as in the NUV, B, R, J and K bands. Their result was that, while type Ia SNe follow the B-band light of their host galaxies, no subclass among them is associated with star formation on time scales of less than a few hundred Myr, ruling out progenitors younger than this for all but a small minority of type Ia events.

4.2.2 Radial distributions of supernovae

Another way to study SN progenitor environments is to use their radial distributions inside their host galaxies. JA06 used a normalized fractional flux method, simply dividing the H α and R-band flux of the part of the galaxy closer to its nucleus than the SN by the total flux. The resulting number, abbreviated as $Fr(\lambda)$ where λ stands for the wavelength band, gives a normalized measure of how far a SN is from the galaxy nucleus *relative to the underlying emission*; $Fr(\lambda) \sim 1$ corresponds to an explosion site outside the galaxy, while $Fr(\lambda) = 0$ corresponds to the nucleus. As with NCR, a population perfectly tracing the galaxy star formation would have a uniform $Fr(\mathrm{H}\ \alpha)$ distribution with a mean of 0.5. JA06 found a lack of type II SNe in central regions of galaxies relative to the H α emission, and considered strong nuclear H α emission not associated with star formation, extinction effects or other biases against detecting type II SNe in nuclear regions. Type Ib/c SNe were found more centrally concentrated than type II, possibly indicating a higher metallicity in their progenitors, as spiral galaxies tend to have metallicity gradients with highest metallicities in the nuclear regions (e.g. Zaritsky et al. 1994). The JA06 analysis was taken further by Anderson & James (2009), Habergham et al. (2010) and Habergham et al. (2012), who employed the same method with larger samples of SNe. Anderson & James (2009) found a similar central deficit of type II SNe and a central excess of type Ibc SNe, attributing these effects to a difference in progenitor metallicity. Habergham et al. (2010) and Habergham et al. (2012), on the other hand, found the central excess of type Ib/c SNe to be more pronounced in 'disturbed' (interacting or showing clear signs of recent interaction) galaxies. They found it difficult to

explain this with a metallicity effect, as disturbed galaxies exhibit a shallow metallicity gradient. They instead proposed a top-heavy IMF in the centers of disturbed galaxies, resulting in larger numbers of massive type Ib/c SN progenitor stars than elsewhere. The results of Habergham et al. (2012) in the R-band are presented in Figure 4.6. This phenomenon could be fueled by a gas inflow caused by the gravitational interaction with another galaxy. Klessen et al. (2007) found that a strong starburst episode could result in a top-heavy IMF.

Radial distances between SNe and host galaxy nuclei have also been analyzed in different ways. Hakobyan (2008) and Hakobyan et al. (2009), for example, normalized the distances between SNe and host galaxy nuclei to R_{25}, the radius at which the surface brightness of the galaxy in a given wavelength band (often B) reaches 25 mag arcsec^{-1}. They then calculated the normalized surface density distributions of different types of SNe. These were assumed to be exponential functions (Barbon et al. 1975; Bartunov et al. 1992) of the form $\Sigma^{SN}(r) = \Sigma_0^{SN} e^{-r/h_{SN}}$, where r is the distance to the nucleus normalized to R_{25} and corrected for effects of inclination, Σ_0^{SN} is the surface density at the galaxy nucleus and h_{SN} is the R_{25}-normalized scale length. They found type Ib/c SNe to be more centrally concentrated (with a shorter normalized scale length) than type II SNe; type Ib/c SNe were additionally found to be unusually concentrated in active (Hakobyan 2008) or very luminous (Hakobyan et al. 2009) galaxies, possibly due to starburst activity in the nuclei. Additionally, no significant difference between types Ib and Ic was found. These results were generally consistent with those from Habergham et al. (2012); however, metallicity differences between progenitors were cited as the favored explanation. Herrero-Illana et al. (2012) applied the method to SNRs and radio SNe in starburst galaxies and luminous infrared galaxies (LIRGs) to infer the presence of nuclear disk structures and a strong excess of SNRs in the nuclear regions of these galaxies. This method can also be used in reverse, to study galaxies using SNe: Hakobyan et al. (2016) studied the effect of a bulge or bar in the host galaxy on the radial distributions of 500 CCSNe and found strong bars to disrupt star formation in the inner regions.

Both of these methods were also employed in Paper I of this thesis, where they were applied to strongly star-forming galaxies. This paper was motivated by the study of Anderson et al. (2011), who found a possibly abnormal population of SNe in the 'SN factory' galaxy system Arp 299, where seven SNe (six CCSNe) have been detected. In Paper I, type Ib/c SNe were

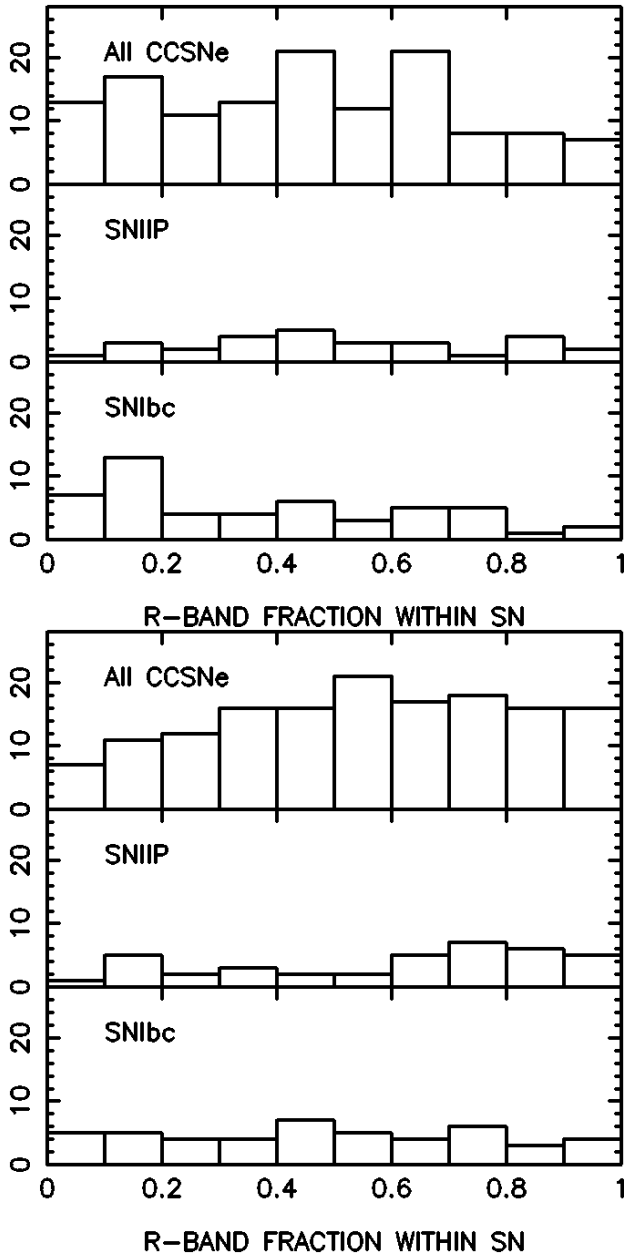

Figure 4.6: Distributions of $Fr(R)$ values from Habergham et al. (2012); 'undisturbed' host galaxies in the upper panel and 'disturbed' ones in the lower panel. An excess of type Ib/c SNe $Fr(R) \leq 0.2$ is visible in 'disturbed' galaxies.

found to be abnormally centralized in strongly star-forming galaxies, possibly as a result of an increased close binary fraction in regions with dense star formation (see also Section 5.1). The dynamical interactions of stars in a dense environment would disrupt binary systems easier than elsewhere, but also bring other binary systems closer together (Heggie 1975).

A caveat needs to be taken into account when discussing radial distribution studies. Mattila et al. (2012) estimated the fractions of missing SNe due to obscuration by host galaxy dust, especially at optical wavelengths. In normal, moderately inclined galaxies, the fraction of missing SNe is between 5 and 36 per cent, while in dusty regions of LIRGs and ultraluminous infrared galaxies (ULIRGs), the missing SNe may constitute as much as 70 or 90 per cent of the total SN population. As an example, SN 2008cs was located in a LIRG and had an extinction of over 15 mag in the V band, but was detected in the NIR (Kankare et al. 2008). SNe close to or coincident with the nuclei of galaxies can also be missed because of inadequate spatial resolution: Mattila et al. (2013) reported two SNe missed by optical surveys in the central regions of the starburst galaxy M 82. This may introduce a bias into the studies comparing the radial distributions of SNe – especially in more dusty actively star-forming galaxies – as type II SNe are intrinsically fainter on average than type Ib/c SNe (Richardson et al. 2014) and thus may be preferentially missed.

4.2.3 Other environmental methods

In addition to the NCR method, associations between SNe and star formation have been studied in other ways. van Dyk (1992) used the distances between SNe and H II regions to confirm the low-mass progenitors of type Ia SNe, but found no significant difference between types II and Ib/c, at least partly because of small number statistics and poor positional accuracy of the locations of some events. van Dyk et al. (1996) confirmed these results with a larger sample and concluded that most type Ib/c progenitors are not WR stars but close binary stars. Crowther (2013) studied the distances between 39 nearby CCSNe (within 15 Mpc) and H II regions using both ground-based and space-based observations of their host galaxies, finding type Ibc SNe more closely associated with star-forming regions than type II. However, 12 of the 18 CCSNe closely associated with star formation were located in or close to giant H II regions, only indicating weak progenitor constraints of $M_{\mathrm{ZAMS}} \geq 12 M_{\odot}$. Aramyan et al. (2016)

instead studied the association between SNe and the spiral arms in their host galaxies. Type Ib/c SNe were found to be located closer to the leading edges of the spiral arms, where star formation is triggered, than type II SNe, indicating more massive progenitors. Type Ia SNe were found to be disconnected from the spiral arms. Galbany et al. (2014) used the equivalent width of the H α line at the explosion sites of SNe and the distances between SNe and H II regions, in addition to the NCR method. Their sample of 81 SN host galaxies was imaged using integral field spectroscopy (IFS), where an entire galaxy can be imaged simultaneously at a range of wavelengths, effectively obtaining a separate spectrum for each pixel. Type Ib/c SNe were found to be more closely associated with star formation than type II regardless of the method used.

Smith et al. (2015) studied the distances between different stars and their nearest massive O-type stars. They found LBV stars to be relatively isolated from O-type stars – and, contrary to expectations, more isolated than WR stars – arguing that LBV stars are kicked mass gainers originating in binary systems instead of a stage of evolution following WR stars. The implication for SNe could be that some type IIn SNe could explode in low-NCR environments while still being the results of LBV evolution. However, Humphreys et al. (2016) pointed out flaws in this argument, including the inclusion of different types of LBVs with different ZAMS masses in their sample. When the LBVs were separated into bins based on luminosity (and likely ZAMS mass), the luminous and massive LBVs were found to be closely associated with O-type stars.

The metallicities of the explosion sites of CCSNe have been examined by e.g. Galbany et al. (2016). They studied a sample of 115 host galaxies with 74 CCSNe and 58 type Ia SNe, observed using IFS, and found the progenitors of type II and Ic SNe to have a higher metallicity than the progenitors of types Ib and IIb. They concluded that at least some type Ic SNe originate in single massive progenitors stripped by metallicity-driven winds. On the other hand, the lower metallicity of type Ib SNe suggests that their progenitors are instead stripped by interaction with a binary companion. This is in line with earlier results by Kelly & Kirshner (2012). Sanders et al. (2012), on the other hand, found the metallicities of type Ib and Ic SNe not to be different enough for metallicity to be the deciding factor between the two. Taddia et al. (2015) studied the metallicities at the sites of interacting transients in particular – type IIn SNe and SN impostors. They found type IIn SNe to have a metallicity distribution consistent with a mixture of

RSG and LBV progenitors (high and low metallicity, respectively), while impostors were found to correspond to LBVs alone. Modjaz et al. (2008) studied the metallicities of type Ic-BL SN sites, and found the events not associated with a GRB to be located in more metal-rich environments.

General properties of host galaxies have also been used to study SN progenitors. Lunnan et al. (2014), for example, found the host galaxies of SLSNe to be similar to those of long GRBs in terms of mass, luminosity, total star formation rate and metallicity. The masses, luminosities and metallicities of these galaxies were found to be significantly lower than those of other CCSN hosts, consistently with earlier results by Neill et al. (2011).

In some cases, even with pre-explosion imaging of a CCSN host galaxy, the progenitor star cannot be pinpointed and instead the source at the SN location is a cluster (this was the case for e.g. SN 2009kr; Maund et al. 2015b). Sometimes no pre-explosion imaging is available, but the stellar population at the SN site can be studied in post-SN high-resolution imaging when the SN no longer contributes significantly to the local brightness. In such cases, stellar population fitting can be used. For example, van Dyk et al. (1999) fitted the Padova group stellar models (Bertelli et al. 1994) to *HST* photometry of the site of SN 1979C and found the progenitor consistent with an initially 17 – 18 $M_{\odot}$ RSG, while Maund et al. (2015b) found the progenitor of SN 2009kr consistent with $M_{\rm ZAMS} \leq 25M_{\odot}$. Both of these SNe were of type II-L. The stellar population of the host association of the type Ic SN 2007gr was used by Maund et al. (2016) to imply an initially $\sim 30M_{\odot}$ progenitor, possibly a WR star. Kuncarayakti et al. (2013a,b) used IFS and stellar population modeling to infer that at least some type II SNe have progenitors similar to those of type Ib/c SNe ($\gtrsim 25M_{\odot}$).

4.3 Nebular spectra

Information about the progenitor of a SN can also be obtained through its late-time spectra. In the nebular phase, when most of the light from a SN is due to emission lines from the ejecta, those lines can be used to estimate ejecta masses and expansion velocities. Synthetic spectra are produced using radiative transfer models, taking into account ejecta heating by γ-rays and positrons from the ^{56}Co decay and cooling by line emission to obtain the temperature and ionization state, with chemical abundances and the ejecta

mass as parameters. These can be compared to the observed spectra to draw conclusions about the chemical abundances and masses in the ejecta. These, in turn, can be compared to stellar evolution and nucleosynthesis models to find the mass and evolutionary path of the progenitor star.

Jerkstrand et al. (2012) studied the nebular spectra of the type II-P SN 2004et. The output was compared to hydrodynamic explosion and nucleosynthesis models by Woosley & Heger (2007). They showed that several lines in the nebular spectra of type II-P SNe are sensitive to the progenitor mass, especially [O I] $\lambda\lambda$6300, 6364, but also Na I $\lambda\lambda$5890, 5896, Mg I] λ4571, along with several NIR lines of carbon, silicon, neon and magnesium. Models at different masses were compared to the nebular spectra and a progenitor mass of 15 $M_\odot$, with 0.8 $M_\odot$ of oxygen, was found to provide the best match. Shivvers et al. (2013) studied the nebular spectra of type IIb SN 2011dh and compared them to a code developed by Mazzali et al. (2001), which takes into account the ^{56}Co decay and line cooling, but ignores recombination emission. In this way, the ^{56}Ni mass of 0.07 $M_\odot$ powering the explosion could be obtained as well. A progenitor mass of 13 – 15 $M_\odot$ was estimated. Jerkstrand et al. (2015) performed a detailed examination of the nebular spectra of type IIb SNe (including SN 2011dh) similarly to Jerkstrand et al. (2012), and found progenitor masses between 12 and 16 $M_\odot$. Generally these results are consistent with direct progenitor detections.

Kuncarayakti et al. (2015) used the [O I] $\lambda\lambda$6300, 6364 line fluxes in particular to estimate an oxygen mass of 0.8 $M_\odot$ for the type Ib SN iPTF13bvn using the Uomoto (1986) relation. In the high-density limit, the minimum mass of oxygen to produce the observed line luminosity depends on the temperature as

$$M_{\mathrm{O}}(M_\odot) = 10^8 f([\mathrm{O\ I}]) D^2 \exp(2.28/T_4), \tag{4.3}$$

where f([O I]) is the line flux in erg s^{-1} cm^{-2}, D is the distance in Mpc and T_4 is the temperature of the oxygen-containing region in units of 10^4 K, which can be estimated from line ratios and has an effect on transition rates. Using several nucleosynthesis models the progenitor mass was estimated as 15 – 17 $M_\odot$, indicating a binary progenitor instead of a single WR star.

Late-time spectra of SLSNe have also been studied. Jerkstrand et al. (2016a) found spectra of slowly-declining type Ic SLSNe SN 2007bi and PTF12dam incompatible with PISN models by Heger & Woosley (2002):

emission lines of oxygen, iron and magnesium not predicted from models with $\geq 65 M_{\odot}$ helium cores were observed. Nicholl et al. (2016b) compared SN 2015bn, another SLSN of the same type, to the Jerkstrand et al. (2016a) spectra to reach the same conclusion, and based on the similarity to less luminous type Ic SNe, its ^{56}Ni mass was found to be too small for its decay to explain the extreme brightness. Jerkstrand et al. (2016b) showed that the late-time spectra of slowly-declining type Ic SLSNe in general require large oxygen ejecta masses ($\gtrsim 10 M_{\odot}$, which is, however, too small for PISN models) and thus are consistent with newborn magnetars from massive WR progenitors ($M_{\mathrm{ZAMS}} \gtrsim 40 M_{\odot}$).

4.4 Supernova searches and rates

Another statistical way to gain information about SN progenitors is to study their relative rates. How these rates change with redshift and host galaxy properties, and how they compare to statistics about stellar masses, binarity and other factors, can help constrain the progenitor systems. However, a caveat worth mentioning is that the relative rates may be skewed by the missed SNe (Dahlen et al. 2012; Mattila et al. 2012). This is not a problem if the fraction of missed SNe is the same for all types, but this is not likely to be the case.

One important source of SN rates is the Lick Observatory Supernova Search (LOSS) project and studies based on it (Li et al. 2011a,c). In these studies, a volume-limited sample of CCSNe was constructed within 60 Mpc; with 106 CCSNe, the completeness within this distance was estimated by Li et al. (2011a) to be ∼80 per cent. Correcting for this incompleteness, the relative rates of SNe were computed. Smith et al. (2011a) discussed the implications of these rates by comparing them to expectations from the IMF and binary fractions. The fraction of SE-SNe ($36.5^{+5.5}_{-5.4}$ per cent of all CCSNe when including type IIb and $26.0^{+5.1}_{-4.8}$ per cent for types Ib/c) was found to be too high to be explained by single WR progenitors, even with overly generous estimates for mass loss efficiency; instead, interacting binary stars in the ZAMS mass range of 8.5 – 25 $M_{\odot}$ were estimated to produce the observed type Ib and IIb SNe. Type Ic SNe were suggested to arise from more massive stars, as the removal of both the hydrogen and helium envelopes would still require line-driven winds even with binary interaction. Scenarios of direct collapse into black holes were disfavored as

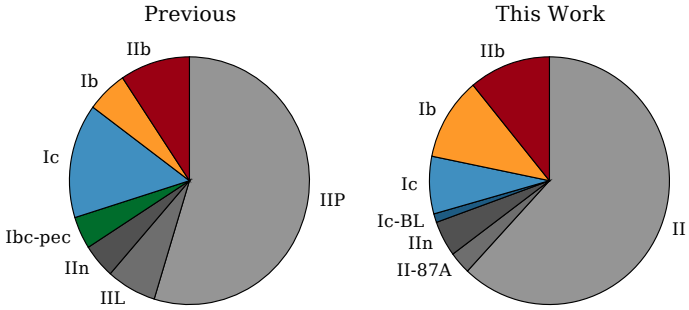

Figure 4.7: Illustration of the updated CCSN rates from Shivvers et al. (2016a) ('this work'), compared to earlier results by Li et al. (2011a) ('previous'). The relative fraction of type Ib has increased significantly, while the fraction of type Ic has decreased and types II-P and II-L are no longer separated.

unnecessary. Eldridge et al. (2013) arrived at only slightly different rates within a 2000 km s^{-1} radial velocity limit, with similar indications for the progenitors.

More recently, the types of some SNe have been updated after a more detailed study (e.g. Modjaz et al. 2014, who found many type Ib events to be mislabeled as Ic), and the LOSS statistics were revisited by Shivvers et al. (2016a). The rates presented earlier in Table 3.1 and illustrated in Figure 4.7 are the updated ones. The new relative rates of type Ib vs. Ic, with type Ib actually being roughly 1.7 times more common than Ic instead of roughly 0.5 times as common (as reported by Smith et al. 2011a), offer even more support to the conclusion that type Ib SNe have lower-mass progenitors than type Ic SNe do.

New high-cadence all-sky transient surveys such as the All-Sky Automated Survey for SuperNovae (ASAS-SN[3]) and large programs dedicated to classifying SNe such as the Public ESO Spectroscopic Survey for Transient Objects (PESSTO[4]) now allow for larger and larger samples of SNe to study their relative rates. In time, such surveys will allow the relative rates of even rarer transients to be constrained.

[3]http://www.astronomy.ohio-state.edu/∼assassin/index.shtml
[4]http://www.pessto.org/

Chapter 5

Summary of the articles

The publications included in this thesis are summarized below. They showcase different observational methods of studying CCSN progenitors, and mostly deal with the environments of CCSN progenitors in some way. Papers I and II concern the environments and statistical distributions of CCSN progenitors in their host galaxies. Paper III describes a case study and proposed progenitor of a particular unusual CCSN, making use of similarities to other CCSNe and an analysis of its environment. In Paper IV, magnetar model fits and late-time spectra are used to infer the progenitor of an unusual SLSN.

In all sections 'we' refers to the authors of the paper in question. My contributions to each paper are summarized at the end of each section.

5.1 Paper I

In Paper I we present a statistical analysis of the environments of CCSNe in strongly star-forming host galaxies. The absorption cross section of dust in the ISM peaks in the UV range, while UV radiation is produced by young stars. The absorbed energy is re-emitted in the far-infrared (FIR) range, making FIR emission a tracer of star formation (Kennicutt 1998)[1]. As such, the galaxies were chosen from among the *IRAS* Revised Bright Galaxy Catalog (Sanders et al. 2003), selected to have a high FIR luminosity (defined here as the luminosity between 40 and 400 μm) of $L_{FIR} > 1.6 \times 10^{10} L_{\odot}$; this is the total FIR luminosity of the NGC 4567/8 galaxy pair. Additionally, the galaxies had to be at a distance of less than 75 Mpc

[1]For starbursts with ages less than 10^8 yr, where the UV and optical emission is dominated by young stars, SFR ($M_{\odot}$ yr^{-1}) $= 4.5 \pm 1.4 \times 10^{-44}$ erg s^{-1}.

and observable from the Roque de los Muchachos Observatory (ORM) at La Palma, resulting in a declination of $\gtrsim -35°$. The sample included 57 galaxies, 22 of which are brighter in FIR than the 'prototypical' starburst galaxy M 82.

The galaxies were observed in the H α line using a narrow-band H α filter and another narrow-band filter in the nearby continuum with the 2.56-m NOT, and in the Ks band with both the NOT and the William Herschel Telescope (WHT); both telescopes are located at the ORM on La Palma. Additionally, NUV images were obtained from the public *GALEX* space telescope data archive. The continuum-filter images were subtracted from the H α images with the ISIS 2.2 package using the Optimal Image Subtraction (OIS) method by Alard & Lupton (1998) and Alard (2000).

The environments of the CCSN sample were analyzed using the NCR method, the JA06 fractional flux method and the Hakobyan et al. (2009) method of calculating the scale length of their surface density distribution. The SE-SNe in the strongly star-forming galaxies in our sample were found to have a shorter scale length than those in normal galaxies, and are thus concentrated closer to the nuclei of their host galaxies, possibly because of an increased close binary fraction in dense regions. No difference was found for type II SNe, which are located further away from the host galaxy nuclei regardless of the star formation rate of the galaxy. The NCR results were mostly consistent with those of Anderson et al. (2012), with the exception of type Ic, whose mean NCR is higher in strongly star-forming galaxies. Type Ib and II progenitors were found similar to each other in terms of mass, with type Ic progenitors being the most massive. The NCR sequence was found in H α, NUV and the NIR Ks band.

I performed roughly half of the observations (the rest being existing data) and the bulk of the optical data reduction. I carried out all of the statistical analysis of the data. As the main author, I contributed the bulk of the material in the paper.

5.2 Paper II

In Paper II we compare the NCR results of Paper I, Anderson et al. (2012) and Habergham et al. (2014) to those of massive stars in order to more quantitatively constrain the CCSN progenitors. Public H α emission maps of two nearby, different galaxies, the irregular LMC and the spiral galaxy

Messier 33 (M33), were obtained. Coordinates of evolved stars in both galaxies were obtained from catalogues, mainly those of RSGs and YSGs (Drout et al. 2012; Neugent et al. 2012) and of WR stars (Bonanos et al. 2009; Neugent & Massey 2011; Hainich et al. 2014). In addition, coordinates of O- and B-type main-sequence stars (corresponding to $\gtrsim 8M_{\odot}$) were obtained from the SIMBAD database. The NCRs of stars were calculated, and the means and distributions of NCR values were compared to those of CCSNe. In addition, systematic effects on the NCR distributions, such as the host galaxy distance, uncertainties in SN coordinates and the addition of noise, were simulated and investigated. The galaxy images were degraded to correspond to the distances of the SN host galaxies in order to make the distributions comparable.

Both main-sequence and evolved stars exhibit a sequence of increasing NCR with increasing ZAMS mass, although the sample of main-sequence stars is most likely spatially biased. The results were mostly found consistent between the LMC and M33, despite the inherent differences such as the masses and metallicities between the galaxies. Type II-P SNe were found to match the distribution of RSGs with $M_{\mathrm{ZAMS}} \gtrsim 9M_{\odot}$, consistently with the established II-P progenitor scenario, thus confirming the validity of the NCR method.

Type Ib SNe were found to be consistent with the same progenitor mass range as type II-P. Type II-L and IIb SNe were both found consistent with higher-mass YSGs, although the sizes of the type IIb and II-L samples result in large uncertainties in their NCRs. The differences between types Ib and II-P on one hand, and between IIb and II-L on the other, are thus indicated to result not from progenitor ZAMS mass differences, but from the presence or lack, respectively, of an interacting binary companion. Type Ic SNe were found consistent with early-type WN stars – WR stars with strong nitrogen features and ZAMS masses of $\gtrsim 20M_{\odot}$. This indicates that the progenitors of type Ic SNe are single WR stars, interacting binary stars of higher ZAMS mass than the progenitors of type Ib SNe, or a mix of both.

I initiated the project, obtained the necessary data from public sources and performed the overwhelming majority of the statistical analysis. As the main author, I contributed the bulk of the material in the paper.

5.3 Paper III

In Paper III we present the results of the follow-up campaign of the unusual, bright type II-L SN 2013fc. This includes optical spectroscopy and photometry covering roughly five months and NIR photometry covering roughly seven months. The classification and follow-up were a part of the PESSTO program, of which I am a member.

Using integral field unit (IFU) spectroscopy of the explosion site, we established that SN 2013fc exploded in a star-forming 'knot' in the circumnuclear ring of its host galaxy, the LIRG ESO 154-G010; using both a stellar population model and a comparison to SN 1998S, we determined this to be a highly reddened region with $A_V = 2.9 \pm 0.2$. The location of SN 2013fc resulted in heavy host galaxy contamination in its spectra and photometry, requiring not only template images but a template spectrum to be subtracted from the images and spectra of the SN. The template images and spectra of the galaxy were observed 1 – 1.5 years after the explosion, when the SN had faded.

Despite an initial classification as type IIn, the light curve of SN 2013fc reveals it as a type II-L SN similar to interacting SNe 1998S (e.g. Fassia et al. 2000, 2001) and 1979C (e.g. de Vaucouleurs et al. 1981; van Dyk et al. 1999), but brighter, with a peak absolute magnitude of $B = -20.46 \pm 0.21$ mag. With an initially featureless blue spectrum, SN 2013fc gradually developed a strong broad (FWHM ~ 8000 km s^{-1}) H α emission line without a P Cygni absorption profile. This is consistent with other type II-L SNe. The similarity to SNe 1998S and 1979C suggests a similar progenitor star; this would mean an extreme RSG with $M_{ZAMS} \sim 17 M_\odot$. A stellar population model was fitted to the SN location, with an estimated age of 10^{+3}_{-2} Myr suggesting $M_{ZAMS} = 19 \pm 4 M_\odot$, which is consistent with the progenitor of SN 1979C.

Signs of dust condensing in a CDS caused by CSM interaction were seen in the NIR photometry. Additionally, the high peak luminosity and the late-phase decline, faster than expected if it was powered by ^{56}Co decay, may be explained by CSM interaction. The similarity to interacting SNe provides further circumstantial evidence of interaction with CSM. Narrow lines from the SN were not detected – if they existed, they would have been completely dominated by the host galaxy contamination. A recent strong RSG wind may be responsible for the mass loss that created this CSM.

I was one of two people who classified SN 2013fc and initiated its follow-

up. I was responsible for the coordination of the optical and NIR follow-up campaign as a part of PESSTO. I reduced a significant part of the photometric and most of the spectroscopic data and performed most of the analysis. As the main author, I contributed the bulk of the material in the paper.

5.4 Paper IV

In Paper IV we describe the follow-up campaign of the hydrogen-poor SLSN Gaia16apd, including optical, UV and NIR photometry and optical spectroscopy, over a period of more than half a year in the rest-frame of the SN. The classification and observations were performed as a part of the NOT Unbiased Transient Survey (NUTS[2]) collaboration.

This event exhibited an unusual early UV brightness (with a peak $M_{uvm2} \simeq -23.6$ mag) and high temperature (> 18000 K) even for a SLSN. Its early optical evolution resembled that of the fast-declining type Ic SLSN SN 2010gx, which may also have evolved similarly in the UV – although there is a lack of early UV data for it and other fast-declining events. Spectroscopically it exhibited the O II absorption lines typical to type Ic SLSNe around 3500 – 4500 Å, and evolved to resemble normal type Ic SNe after maximum light. At late times, the decline time-scale and rate are between fast- and slowly-declining type Ic SLSNe, making Gaia16apd a link between the two subclasses. Another intermediate event, LSQ12dlf, was also identified in the literature. The host galaxy of Gaia16apd is faint and metal-poor, like those of other SLSNe of this type. A public *HST* far-UV spectrum was used to constrain the extinction in the host galaxy to $E(B-V)_{\rm host} = 0.010 \pm 0.005$ mag.

Yan et al. (2016) excluded a PISN scenario as the power source of Gaia16apd based on its UV spectra. As such, magnetar spin-down models described by Kasen & Bildsten (2010) were fitted to the pseudo-bolometric light curve of the SLSN. The transient was found consistent with the birth of a magnetar with a period of $P = 1.9 \pm 0.2$ ms and a magnetic field of $B = 1.9 \pm 0.2 \times 10^{14}$ G, with an ejecta mass of 8 – 16 $M_\odot$, depending on opacity, for the SN itself. The high early UV luminosity is consistent with the heating power expected from such a magnetar.

A comparison between the late-time spectra of Gaia16apd and the

[2]http://csp2.lco.cl/not/

slowly-declining event PTF12dam (Nicholl et al. 2013) revealed a striking spectroscopic similarity between these SLSNe, apart from a faster temperature evolution for Gaia16apd, despite the differences in their photometric evolution. This points toward a similar progenitor scenario for both classes of events. Jerkstrand et al. (2016b) showed that the late spectra of slowly-declining type Ic SLSNe require large oxygen ejecta masses ($\gtrsim 10 M_{\odot}$) and thus massive WR progenitors ($M_{\mathrm{ZAMS}} \gtrsim 40 M_{\odot}$); such a progenitor is consistent with Gaia16apd as well.

I classified Gaia16apd and was responsible for most of the coordination of the optical and NIR follow-up campaign as a part of the NUTS program. I reduced a part of the photometric and all of the spectroscopic data and performed most of the analysis. As the main author, I contributed the bulk of the material in the paper.

Chapter 6

Future work

With the new all-sky surveys replacing targeted SN searches, thousands of SNe are being discovered each year, including peculiar events in unexpected locations. SNe can be caught very young much more reliably than before, yielding important information about the early phases. Future telescopes such as the *James Webb Space Telescope* (*JWST*, a 6.5-m infrared space telescope planned for launch in late 2018) and the Large Synoptic Survey Telescope (LSST, an 8.2-m telescope designed specifically to map the entire sky in a few days, scheduled for the early 2020s) will further improve our ability to detect fainter, more distant events in larger numbers and in a less biased manner.

It is difficult for the direct progenitor detections to keep up with this surge of data, however, as the method requires particularly powerful telescopes, nearby SNe and a confirmation of the disappearance of the progenitor star. Although follow-up campaigns of SNe will continue to be a reliable source of information on individual SNe, statistical methods capable of dealing with large samples are expected to rise in importance. In this light, I aim to continue my work with environmental and statistical studies of CCSN progenitors using the tools developed during my earlier projects. For example, an ongoing project deals with extending the NCR method to normal galaxies in the NIR.

One interesting future development is the Javalambre Physics of the Accelerating Universe Astrophysical Survey (J-PAS), which aims to map over 8000 square degrees of the sky in 56 narrow-band filters. This survey will make it possible to map H α emission – among other spectral lines – in thousands of galaxies at different redshifts and, in conjunction with the new SN discoveries, increase NCR and radial distribution statistics by an order of magnitude. This will allow us to extend both methods to rarer subtypes

of SNe as well as to better quantify the effects of host galaxy properties. The project will be undertaken in collaboration with several researchers from multiple countries. This survey will take a few years to complete. A preliminary survey, the Javalambre Photometric Local Universe Survey (J-PLUS), is already underway, and will provide maps of the same area of the sky, albeit with broader and fewer filters. I will take this opportunity to expand on my environmental studies in the coming years.

In addition, the public VISTA survey of the Magellanic Clouds system (VMC[1]) is in the process of mapping both Magellanic Clouds using the ESO-operated Visible and Infrared Survey Telescope for Astronomy (VISTA), and is nearing completion. I am a member of the survey team. We have initiated a project, in collaboration with researchers from the universities of Cambridge and Dublin, that will allow us to construct an unbiased catalog of massive main sequence stars in the LMC and determine their probable masses based on VISTA NIR photometry and stellar evolution models. This will improve the mass constraints corresponding to different NCR values, and thus further improve the precision of the NCR method. A pilot study for this project using a cluster of stars with spectroscopically determined spectral classes is underway.

[1] http://star.herts.ac.uk/∼mcioni/vmc/

Bibliography

Adams, S. M., Kochanek, C. S., Gerke, J. R., Stanek, K. Z., & Dai, X. 2016a, eprint arXiv:1609.01283, submitted to MNRAS

Adams, S. M., Kochanek, C. S., Gerke, J. R., & Stanek, K. Z. 2016b, eprint arXiv:1610.02402, submitted to MNRAS

Aglietta, M., Badino, G., Bologna, G. et al. 1987, Helvetica Physica Acta, 60, 619

Alard, C. 2000, A&AS, 144, 363

Alard, C., & Lupton, R. H. 1998, ApJ, 503, 325

Aldering, G., Humphreys, R. M., & Richmond, M. 1994, AJ, 107, 662

Anderson, J. P., & James, P. A. 2008, MNRAS, 390, 1527

Anderson, J. P., & James, P. A. 2009, MNRAS, 399, 559

Anderson, J. P., Habergham, S. M., & James, P. A. 2011, MNRAS, 416, 567

Anderson, J. P., Habergham, S. M., James, P. A., & Hamuy, M. 2012, MNRAS, 424, 1372

Anderson, J. P., González-Gaitán, S., Hamuy, M. et al. 2014, ApJ, 786, 67

Anderson, J. P., James, P. A., Förster, F. et al. 2015, MNRAS, 448, 732

Aramyan, L. S., Hakobyan, A. A., Petrosian, A. R. et al. 2016, MNRAS, 459, 3130

Arcavi, I., Gal-Yam, A., Cenko, S. B. et al. 2012, ApJL, 756, L30

Arcavi, I., Gal-Yam, A., Sullivan, M. et al. 2014, ApJ, 793, 38

Arnett, W. D. 1982, ApJ, 253, 785

Baade, W., & Zwicky, F. 1934, Proceedings of the National Academy of Sciences of the United States of America, 20, 259

Barbon, R., Capaccioli, F., & Ciatti, F. 1975, A&A, 44, 267

Barbon, R., Ciatti, F., & Rosino L. 1979, A&A, 75, 287

Barbon, R., Ciatti, F., & Rosino L. 1982, A&A, 116, 35

Barbon, R., Cappellaro, E., & Turatto, M. 1984, A&A, 135, 27

Barkat, Z., Rakavy, G., & Sack, N. 1967, Physical Review Letters, 18, 379

Bartunov, O. S., Makarova, I. N., & Tsvetkov, D. Iu. 1992, A&A, 264, 428

Beasor, E. R., & Davies, B. 2016, MNRAS, 463, 1269

Benetti, S., Cappellaro, E., Turatto, M. et al. 2006, ApJ, 653, L129

Benetti, S., Turatto, M., Valenti, S. et al. 2011, MNRAS, 411, 2726

van den Bergh, S., & Tammann, G. A. 1991, ARA&A, 29, 363

Bertelli, G., Bressan, A., Chiosi, C., Fagotto, F., & Nasi, E. 1994, A&AS, 106, 275

Blinnikov, S. I., & Bartunov, O. S. 1993, A&A, 273, 106

Blondin, J. M., Mezzacappa, A., & DeMarino, C. 2003, ApJ, 584, 971

Bonanos, A. Z., Massa, D.L., Sewilo, M. et al. 2009, AJ, 138, 1003

Botticella, M. T., Pastorello, A., Smartt, S. J. et al. 2009, MNRAS, 398, 1041

Bouchet, P., Phillips, M. M., Suntzeff, N. B. et al. 1991, A&A, 245, 490

Buta, R. J. 1982, PASP, 94, 578

Cao, Y., Kasliwal, M., Arcavi, I. et al. 2013, ApJL, 775, L7

di Carlo, E., Massi, F., Valentini, G. et al. 2002, ApJ, 573, 144

Catchpole, R. M., Menzies, J. W., Monk, A. S. et al. 1987, MNRAS, 229, 15P

Chen, J., Wang, X., Ganeshalingam, M. et al. 2014, ApJ, 790, 120

Chevalier, R. A., & Fransson, C. 1994, ApJ, 420, 268

Chugai, N. N. 2001, MNRAS, 326, 1448

Chugai, N. N., Blinnikov, S., Cumming, R. J. et al. 2004, MNRAS, 352, 1213

Colgate, S. A., Petschek, A, G., & Kriese, J. T. 1980, ApJ, 237, L81

Crockett, R. M., Smartt, S. J., Eldridge, J. J. et al. 2007, MNRAS, 381, 835

Crowther, P. A. 2007, ARA&A, 45, 177

Crowther, P. A. 2013, MNRAS, 428, 1927

Dahlen, T., Strolger, L.-G., Riess, A. G. et al., 2012, ApJ, 757, 70

Dessart, L., Hillier, D. J., Gezari, S., Basa, S., & Matheson, T. 2009, MNRAS, 394, 21

Dessart, L., Waldman, R., Livne, E., Hillier, D. J., & Blondin, S. 2013, MNRAS, 428, 3227

Dilday, B., Howell, D. A., Cenko, S. B. et al. 2012, Science, 337, 942

Dong, S., Shappee, B. J., Prieto, J. L. et al. 2016, Science, 351, 257

Drout, M. R., Massey, P., & Meynet, G. 2012, ApJ, 750, 97

Duncan, R. C., & Thompson, C. 1992, ApJ, 392, L9

van Dyk, S. D. 1992, AJ, 103, 1788

van Dyk, S. D., & Matheson, T. 2012, ApJ, 746, 179

van Dyk, S. D., Hamuy, M., & Filippenko, A.V. 1996, AJ, 111, 2017

van Dyk, S. D., Peng, C. Y., Barth, A. J. et al. 1999, PASP, 111, 313

van Dyk, S. D., Peng, C. Y., King, J. Y. et al. 2000, PASP, 112, 1532

van Dyk, S. D., Li, W., Cenko, S. B. et al. 2011, ApJ, 741, L28

van Dyk, S. D., Zheng, W., Fox, O. D. et al. 2014, AJ, 147, 37

van Dyk, S. D., de Mink, S. E., & Zapartas, E. 2016, ApJ, 818, 75

Ekström, S., Georgy, C., Eggenberger, P. et al. 2012, A&A, 537, A146

Eldridge, J. J., & Maund, J. R. 2016, MNRAS, 461, L117

Eldridge, J. J., & Tout, C. A. 2004, MNRAS, 353, 87

Eldridge, J. J., Izzard, R. G., & Tout, C. A. 2008, MNRAS, 384, 1109

Eldridge, J. J., Fraser, M., Smartt, S. J., Maund, J. R., & Crockett, R. M. 2013, MNRAS, 436, 774

Elias-Rosa, N., van Dyk, S. D., Li, W. et al. 2011, ApJ, 742, 6

Elmhamdi, A., Danziger, I. J., Chugai, N. et al. 2003, MNRAS, 338, 939

Ergon, M., Sollerman, J., Fraser, M. et al. 2014, A&A, 562, A17

Ertl, T., Janka, H.-Th., Woosley, S. E., Sukhbold, T., & Ugliano, M. 2016, ApJ, 818, 124

Faran, T., Poznanski, D., Filippenko, A. V. et al. 2014, MNRAS, 445, 554

Fassia, A., Meikle, W. P. S., Vacca, W. D. et al. 2000, MNRAS, 318, 1093

Fassia, A., Meikle, W. P. S., Chugai, N. et al. 2001, MNRAS, 325, 907

Filippenko, A. V. 1997, ARA&A, 35, 309

Filippenko, A. V., Richmond, M. W., Matheson, T. et al. 1992, ApJL, 384, L15

Filippenko, A. V., Matheson, T., & Ho, L. C. 1993, ApJL, 415, L103

Filippenko, A. V., Barth, A. J., Matheson, T. et al. 1995, ApJL, 450, L11

Folatelli, G., Bersten, M. C., Benvenuto, O. G. et al. 2014, ApJL, 793, L22

Folatelli, G., Bersten, M. C., Kuncarayakti, H. et al. 2015, ApJ, 811, 147

Folatelli, G., van Dyk, S. D., Kuncarayakti, H. et al. 2016, ApJL, 825, L22

Foley, R. J., Challis, P. J., Chornock, R. et al. 2013, ApJ, 767, 57

Fox, O. D., Azalee Bostroem, K., van Dyk, S. D. et al. 2014, ApJ, 790, 17

Fox, O. D., Silverman, J. M., Filippenko, A. V. et al. 2015a, MNRAS, 447, 772

Fox, O. D., Smith, N., Ammons, S. M. et al. 2015b, MNRAS, 454, 4366

Fransson, C., Challis, P. J., Chevalier, R. A. et al. 2005, ApJ, 622, 991

Fransson, C., Ergon, M., Challis, P. J. et al. 2014, ApJ, 797, 118

Fransson, C., Larsson, J., Migotto, K. et al. 2015, ApJL, 806, L19

Fraser, M. 2016, MNRAS, 456, L16

Fraser, M., Maund, J. R., Smartt, S. J. et al. 2012, ApJL, 759, L13

Fraser, M., Kotak, R., Pastorello, A. et al. 2015, MNRAS, 453, 3886

Fruchter, A. S., Leva, A. J., Strolger, L. et al. 2006, Nature, 441, 463

Fryer, C. L. 1999, ApJ, 522, 413

Gaensler, B. M., McClure-Griffiths, N. M., Oey, M. S. et al. 2005, ApJ, 620, L95

Galbany, L., Stanishev, V., Mourão, A. M. et al. 2014, A&A, 572, A38

Galbany, L., Stanishev, V., Mourão, A. M. et al. 2016, A&A, 591, A48

Gal-Yam, A., & Leonard, D. C. 2009, Nature, 458, 865

Gal-Yam, A., Mazzali, P., Ofek, E. et al. 2009, Nature, 462, 624

Gal-Yam, A. 2012, Science, 337, 927

Gaskell, C. M., Cappellaro, E., Dinerstein, H. L., Garnett, D. R., Harkness, R. P., & Wheeler, J. C. 1986, ApJ, 306, L77

Gezari, S., Halpern, J. P., Komossa, S. Grupe, D., & Leighly, K. M. 2003, ApJ, 592, 42

Gezari, S., Halpern, J. P., Grupe, D. et al. 2009, ApJ, 690, 1313

Gogarten, S. M., Dalcanton, J. J., Williams, B. F. et al. 2009, ApJ, 691, 115

Gorbikov, E., Gal-Yam, A., Ofek, E. O. et al. 2014, MNRAS, 443, 671

Grassberg, E. K., Imshennik, V. S., & Nadyozhin, D. K., 1971, Ap&SS, 10, 28

Groh, J. H., Georgy, C., & Ekström, S. 2013a, A&A, 558, L1

Groh, J. H., Meynet, G., Georgy, C., & Ekström, S. 2013b, A&A, 558, A131

Habergham, S. M., Anderson, J. P., & James, P. A. 2010, ApJ, 717, 342

Habergham, S. M., James, P. A., & Anderson, J. P. 2012, MNRAS, 424, 2841

Habergham, S. M., Anderson, J. P., James, P. A., & Lyman, J. D. 2014, MNRAS, 441, 2230

Hainich, R., Rühling, U., Todt, H. et al. 2014, A&A, 565, A27

Hakobyan, A. A. 2008, Astrophysics, 51, 69

Hakobyan, A. A., Mamon, A., Petrosian, A. R., Kunth, D., & Turatto, M. 2009, A&A, 508, 1259

Hakobyan, A. A., Karapetyan, A. G., Barkhudaryan, L. V. et al. 2016, MNRAS, 456, 2848

Hamuy, M., Pinto, P. A., Maza, J. et al. 2001, ApJ, 558, 615

Heger, A., & Woosley, S. E. 2002, ApJ, 567, 532

Heger, A., Fryer, C. L., Woosley, S. E., Langer, N., & Hartmann, D. H. 2003, ApJ, 591, 288

Heggie, D. C. 1975, MNRAS, 173, 729

Hendry, M. A., Smartt, S. J., Crockett, R. M. et al. 2006, MNRAS, 369, 1303

Herrero-Illana, R., Pérez-Torres, M. A., & Alberdi, A. 2012, A&A, 540, L5

Horiuchi, S., Nakamura, K., Takiwaki, T., Kotake, K., & Tanaka, M. 2014, MNRAS, 445, L99

Howell, D. A., Sullivan, M., Nugent, P. E. et al. 2006, Nature, 443, 308

Hoyle, F., & Fowler, W. A. 1960, ApJ, 132, 565

Humphreys, R. M., & Davidson, K. 1994, PASP, 106, 1025

Humphreys, R. M., Weis, K., Davidson, K., & Dorgon, M. S. 2016, ApJ, 825, 64

Iben, I. Jr., & Tutukov, A. V., 1984, ApJS, 54, 335

Inserra, C., & Smartt, S. J. 2014, ApJ, 796, 87

Inserra, C., Smartt, S. J., Jerkstrand, A. et al. 2013, ApJ, 770, 128

Inserra, C., Fraser, M., Smartt, S. J. et al. 2016a, MNRAS, 459, 2721

Inserra, C., Smartt S. J., Gall, E. E. E. 2016b, eprint arXiv:1604.01226, submitted to ApJ

Iwamoto, K., Mazzali, P. A., Nomoto, K. et al. 1998, Nature, 395, 672

James, P. A., & Anderson, J. P. 2006, A&A, 453, 57

Janka, H.-Th., Langanke, K., Marek, A., Martínez-Pinedo, G., & Müller, B. 2007, PhR, 442, 38

Jerkstrand, A., Fransson, C., Maguire, K. et al. 2012, A&A, 546, A28

Jerkstrand, A., Ergon, M., Smartt, S. J. et al. A&A, 573, A12

Jerkstrand, A., Smartt, S. J., & Heger, A. 2016a, MNRAS, 455, 3207

Jerkstrand, A., Smartt, S. J., Inserra, C. et al. 2016b, eprint arXiv:1608.02994, submitted to ApJ

Jones, S., Röpke, F. K., Pakmor, R. et al. 2016, A&A, 593, A72

Kankare, E., Mattila, S., Ryder, S. et al. 2008, ApJL, 689, L97

Kankare, E., Ergon, M., Bufano, F. et al. 2012, MNRAS, 424, 855

Kankare, E., Kotak, R., Pastorello, A. et al. 2015, A&A, 581, L4

Kasen, D. 2006, ApJ, 649, 939

Kasen, D., & Bildsten, L. 2010, ApJ, 717, 245

Kasen, D., Woosley, S. E., & Heger, A. 2011, ApJ, 734, 102

Kasliwal, M. M., 2011, Bridging the gap: elusive explosions in the local universe, thesis (Ph.D.) – California Institute of Technology, 2011. Advisor(s): Kulkarni, Shrinivas R.

Kelly, P. L., & Kirshner, R. P. 2012, ApJ, 759, 107

Kelly, P. L., Fox, O. D., Filippenko A. V. et al. 2014, ApJ, 790, 3

Kennicutt, R. C. Jr. 1998, ARA&A, 36, 189

Khokhlov, A. M. 1991, A&A, 245, 114

Kilpatrick, C. D., Andrews, J. E., Smith, N. et al. 2016, MNRAS, 463, 1088

Kippenhahn, R., Weigert, A., & Weiss, A. 2012, *Stellar Structure and Evolution*, Second Edition, Springer

Klessen, R. S., Spaans, M., & Jappsen, A.-K. 2007, MNRAS, 374, L29

Kobulnicky, H. A., & Fryer, C. L. 2007, ApJ, 670, 747

Kouvetouliou, C., Dieters, S., Strohmayer, T. et al. 1998, Nature, 393, 235

Kouvetouliou, C., Strohmayer, T., Hurley, K. et al. 1999, ApJ, 510, L115

Kuncarayakti, H., Doi, M., Aldering, G. et al. 2013a, AJ, 146, 30

Kuncarayakti, H., Doi, M., Aldering, G. et al. 2013b, AJ, 146, 31

Kuncarayakti, H., Maeda, K., Bersten, M. C. et al. 2015, A&A, 579, A95

Langer, N. 2012, ARA&A, 50, 107

Leibundgut, B., Kirshner, R. P., Phillips, M. M. et al. 1993, AJ, 105, 301

Leloudas, G., Fraser, M., Stone, N. C. et al. 2016, NatAs, 1, 0002

Li, W., Leaman, J., Chornock, R. et al. 2011a, MNRAS, 412, 1441

Li, W., Bloom, J. S., Podsiadlowski, Ph. et al. 2011b, Nature, 480, 348

Li, W., Chornock, R., Leaman, J. et al. 2011c, MNRAS, 412, 1473

Liu, Y.-Q., & Modjaz, M. 2016, eprint arXiv:1612.07321, submitted to ApJ

Livne, E. 1990, ApJ, 354, L53

Lovegrove, E., & Woosley, S. E. 2013, ApJ, 769, 109

Lundqvist, P., Nyholm, A., Taddia, F. et al. 2015, A&A, 577, A39

Lunnan, R., Chornock, R., Berger, E. et al. 2014, ApJ, 787, 138

Lunnan, R., Chornock, R., Berger, E. et al. 2016, ApJ, 831, 144

Lyman, J. D., Bersier, D., James, P. A. et al. 2016, MNRAS, 457, 328

Maeda, K., Katsuda, S., Bamba, A., Terada, Y., & Fukazawa, Y. 2014, ApJ, 785, 95

Maeda, K., Hattori, T., Milisavljevic, D. et al. 2015, ApJ, 807, 35

Maeder, A. 1981, A&A, 99, 97

Maoz, D., & Mannucci, F. 2011, PASA, 29, 447

Maoz, D., Mannucci, F., & Nelemans, G. 2014, ARA&A, 52, 107

Mattila, S., Meikle, W. P. S., Lundqvist, P. et al. 2008, MNRAS, 389, 141

Mattila, S., Smartt, S. J., Eldridge, J. J. et al. 2008, ApJ, 688, L91

Mattila, S., Dahlen, T., Efstathiou, A. et al. 2012, ApJ, 756, 111

Mattila, S., Fraser, M., Smartt, S. J. et al. 2013, MNRAS, 431, 2050

Mauerhan, J.C., van Dyk, S. D., Johansson, J. et al. 2016, eprint arXiv:1611.07930, accepted for publication in ApJ

Maund, J. R., & Ramirez-Ruiz, E. 2016, MNRAS, 456, 3175

Maund, J. R., Smartt, S. J., Kudritzki, R.-P., Podsiadlowski, Ph., Gilmore, G. F. 2004, Nature, 427, 129

Maund, J. R., Smartt, S. J., Kudritzki, R.-P. et al. 2006, MNRAS, 369, 390

Maund, J. R., Fraser, M., Ergon, M. et al. 2011, ApJL, 739, L37

Maund, J. R., Mattila, S., Ramirez-Ruiz, E., & Eldridge, J. J. 2014, MNRAS, 438, 1577

Maund, J. R., Arcavi, I., Ergon, M. et al. 2015a, MNRAS, 454, 2580

Maund, J. R., Fraser, M., Reilly, E., Ergon, M., & Mattila, S. 2015b, MNRAS, 447, 3207

Maund, J. R., Pastorello, A., Mattila, M., Itagaki, K., & Boles, T. 2016, ApJ, 833, 128

Mazzali, P. A., Nomoto, K., Patat, F., & Maeda, K. 2001, ApJ, 559, 1047

McCray, R., & Fransson, C. 2016, ARA&A, 54, 19

McCrum, M., Smartt, S. J., Kotak, R. et al. 2014, MNRAS, 437, 656

McCrum, M., Smartt, S. J., Rest, A. et al. 2015, MNRAS, 448, 1206

Menzies, J. W., Catchpole R. M., van Vuuren, G. et al. 1987, MNRAS, 227, 39P

Milisavljevic, D., Margutti, R., Parrent, J. T. et al. 2015, ApJ, 799, 51

de Mink, S. E., Sana, H., Langer, N., Izzard, R. G., & Schneider, F. R. N. 2014, ApJ, 782, 7

Minkowski, R. 1941, PASP, 53, 224

Miyaji, S., Nomoto, K., Yokoi, K., & Sugimoto, D. 1980, PASJ, 32, 303

Modjaz, M., Kewley, L., Kirshner, R. P. et al. 2008, AJ, 135, 1136

Modjaz, M., Blondin, S., Kirshner, R. P. et al. 2014, AJ, 147, 99

Moriya, T. J., & Eldridge, J. J. 2016, MNRAS, 461, 2155

Moriya, T. J., & Maeda, K. 2016, ApJ, 824, 100

Moriya, T. J., Tominaga, N., Langer, N. et al. 2014, A&A, 569, A57

Moriya, T. J., Liu, Z.-W., Mackey, J., Chen, T.-W., & Langer, N. 2015, A&A, 584, L5

Morris, T., & Podsiadlowski, Ph. 2009, MNRAS, 399, 515

Nakar, E., & Piro, A. 2014, ApJ, 788, 193

Neill, J. D., Sullivan, M., Gal-Yam, A. et al. 2011, ApJ, 727, 15

Neugent, K. F., & Massey, P. 2011, ApJ, 733, 123

Neugent, K. F., Massey, P., Skiff, B., & Meynet, G. 2012, ApJ, 749, 177

Nicholl, M., & Smartt, S. J. 2016, MNRAS, 457, L79

Nicholl, M., Smartt, S. J., Jerkstrand, A. et al. 2013, Nature, 502, 346

Nicholl, M., Smartt, S. J., Jerkstrand, A. et al. 2014, MNRAS, 444, 2096

Nicholl, M., Smartt, S. J., Jerkstrand, A. et al. 2015, MNRAS, 452, 3869

Nicholl, M., Berger, E., Smartt, S. J. et al. 2016a, ApJ, 826, 39

Nicholl, M., Berger, E., Margutti, R. et al. 2016b, ApJL, 828, L18

Nomoto, K. 1982, ApJ, 253, 798

Nomoto, K. 1984, ApJ, 277, 791

Nomoto, K. 1987, ApJ, 322, 206

Nomoto, K., Mazzali, P. A., Nakamura, T. et al. 2001, Supernovae and gamma-ray bursts: the greatest explosions since the Big Bang. Proceedings of the Space Telescope Science Institute Symposium, held in Baltimore, MD, USA, May 3 - 6, 1999, edited by Mario Livio, Nino Panagia, Kailash Sahu. Space Telescope Science Institute symposium series, Vol. 13., 144

Nomoto, K., Tominaga, N., Tanaka, M., & Maeda, K. 2007, The multicolored landscape of compact objects and their explosive origins, AIP Conference Proceedings, 924, 108

Ofek, E. O., Cameron, P. B., Kasliwal, M. M. et al. 2007, ApJ, 659, L13

O'Connor, E., & Ott, C. D. 2011, ApJ, 730, 70

Okyudo, M., Kato, T., Ishida, T., Tokimasa, N., & Yamaoka, H. 1993, PASJ, 45, L63

Paczyński, B. 1967, Acta Astronomica, 17, 355

Parrent, J. T., Howell, D. A., Friesen, B. et al. 2012, ApJL, 752, L26

Pastorello, A., Smartt, S. J., Mattila, S. et al. 2007, Nature, 447, 829

Pastorello, A., Kasliwal, M. M., Crockett, R. M. et al. 2008a, MNRAS, 389, 955

Pastorello, A., Mattila, S., Zampieri, L. et al. 2008b, MNRAS, 389, 113

Pastorello, A., Quimby, R. M., Smartt, S. J. et al. 2008c, MNRAS, 389, 131

Pastorello, A., Smartt, S. J., Botticella, M. T. et al. 2010, ApJL, 724, L16

Pastorello, A., Pumo, M. L., Navasardyan, H. et al. 2012, A&A, 537, 141

Pastorello, A., Cappellaro, E., Inserra, C. et al. 2013, ApJ, 767, 1

Pastorello, A., Benetti, S., Brown, P. J. et al. 2015a, MNRAS, 449, 1921

Pastorello, A., Prieto, J. L., Elias-Rosa, N. et al. 2015b, MNRAS, 453, 3649

Pastorello, A., Wang, X.-F., Ciabattari, F. et al. 2016, MNRAS, 456, 853

Pejcha, O., & Thompson, T. A. 2015, ApJ, 801, 90

Pérez-Torres, M. A., Lundqvist, P., Beswick, R. J. et al. 2014, ApJ, 792, 38

Perlmutter, S., Aldering, G., Goldhaber, G. et al. 1999, ApJ, 517, 565

Perley, D. A., Quimby, R. M., Yan, L. et al. 2016, ApJ, 830, 13

Perryman, M. A. C., Lindegren, L., Kovalevsky, J. et al. 1997, A&A, 323, L49

Phillips, M. M., 1993, ApJ, 413, L105

Piran, T. 2004, Reviews of Modern Physics, 76, 1143

Podsiadlowski, Ph., Joss, P. C., & Hsu, J. J. L. 1992, ApJ, 391, 246

Podsiadlowski, Ph., Hsu, J. J. L., Joss, P. C., & Ross, R. R. 1993, Nature, 364, 509

Prajs, S., Sullivan, M., Smith, M. et al. 2017, MNRAS, 464, 3568

Quimby, R. M., Aldering, G., Wheeler, J. C. et al. 2007, ApJ, 668, L99

Quimby, R. M., Kulkarni, S. R., Kasliwal, M. M., 2011, Nature, 474, 487

Quimby, R. M., Yuan, F., Akerlof, C., & Wheeler, J. C. 2013, MNRAS, 431, 912

Rees, M. J. 1988, Nature, 333, 523

Reynolds, T. M., Fraser, M., & Gilmore, G. 2015, MNRAS, 453, 2885

Richardson, D., Jenkins, R. L. III, Wright, J., & Maddox, L. 2014, AJ, 147, 118

Richmond, M. W., van Dyk, S. D., Ho, W. et al. 1996, AJ, 111, 327

Riess, A. G., Filippenko, A. V., Challis, P. et al. 1998, AJ, 116, 1009

Roy, R., Kumar, B., Maund, J. R. et al. 2013, MNRAS, 434, 2032

Sana, H., de Mink, S. E., de Koter, A. et al. 2012, Science, 337, 444

Sanders, D. B., Mazzarella, J. M., Kim D.-C., Surace J. A., & Soifer, B. T. 2003, AJ, 126, 1607

Sanders, D. B., Soderberg, A. M., Levesque, E. M. et al. 2012, ApJ, 758, 132

Sanders, N. E., Soderberg, A. M., Gezari, S. et al. 2015, ApJ, 799, 208

Savaglio, S., Glazebrook, K., & Le Borgne, D. 2009, ApJ, 691, 182

Schlegel, E. M. 1990, MNRAS, 244, 269

Schlegel, E. M. 1996, AJ, 111, 1660

Schulze, S., Krühler, T., Leloudas, G. et al. 2016, eprint arXiv:1612.05978

Shigeyama, T., Suzuki, T., Kumagai, S. et al. 1994, ApJ, 420, 341

Shivvers, I., Mazzali, P., Silverman, J. M. et al. 2013, MNRAS, 436, 3614

Shivvers, I., Modjaz, M., Weikang, Z. et al. 2016a, eprint arXiv:1609.02922, accepted for publication in PASP

Shivvers, I., Zheng, W. K., Mauerhan, J. C. et al. 2016b, MNRAS, 461, 3057

Siess, L. 2007, A&A, 476, 893

Smartt, S. J. 2009, ARA&A, 47, 63

Smartt, S. J. 2015, PASA, 32, e016

Smith, N. 2013, MNRAS, 434, 102

Smith, N. 2014, ARA&A, 52, 487

Smith, N., & Tombleson, R. 2015, MNRAS, 447, 598

Smith, N., Li, W., Foley, R. J. et al. 2007, ApJ, 666, 1116

Smith, N., Li, W., Filippenko, A. V., & Chornock, R. 2011a, MNRAS, 412, 1522

Smith, N., Li, W., Miller, A. A. et al. 2011b, ApJ, 732, 63

Smith, N., Li, W., Silverman, J. M., Ganeshalingam, M., & Filippenko, A. V. 2011c, MNRAS, 415, 773

Smith, N., Mauerhan, J. C., Silverman, J. M., 2012, MNRAS, 426, 1905

Smith, N., Mauerhan, J. C., & Prieto, J. L. 2014, MNRAS, 438, 1191

Smith, N., Mauerhan, J. C., Cenko, S. B. et al. 2015, MNRAS, 449, 1876

Soderberg, A. M., Nakar, E., Berger, E., & Kulkarni, S. R. 2006, ApJ, 638, 930

Sollerman, J., Cumming, R., & Lundqvist, P. 1998, ApJ, 493, 933

Srivastav, S., Ninan, J. P., Kumar, B. et al. 2016, MNRAS, 457, 1000

Sundqvist, J. O., & Owocki, S. P. 2013, MNRAS, 428, 1837

Taddia, F., Stritzinger, M. D., Sollerman, J. et al. 2013a, A&A, 555, A10

Taddia, F., Stritzinger, M. D., Sollerman, J. et al. 2013b, A&A, 555, A10

Taddia, F., Sollerman, J., Fremling, C. et al. 2015, A&A, 580, A131

Taddia, F., Fremling, C., Sollerman, J. et al. 2016, A&A, 592, A89

Takáts, K., Pignata, G., Bersten, M. et al. 2016, MNRAS, 460, 3447

Tartaglia, L., Pastorello, A., Taubenberger, S. et al. 2015, MNRAS, 447, 117

Tartaglia, L., Elias-Rosa, N., Pastorello, A. et al. 2016,a ApJL, 823, L23

Tartaglia, L., Pastorello, A., Sullivan, M. et al. 2016b, MNRAS, 459, 1039

Tartaglia, L., Fraser, M., Sand, D. J. et al. 2016c, eprint arXiv:1611.00419, submitted to ApJ Letters

Terreran, G., Jerkstrand, A., Benetti, S. et al. 2016, MNRAS, 462, 137

Tolstov, A., Nomoto, K., Blinnikov, S. et al. 2016, eprint arXiv:1612.01634, accepted for publication in ApJ

Tominaga, N., Blinnikov, S., & Nomoto, K. 2013, ApJL, 771, L12

Trundle, C., Kotak, R., Vink, J. S., & Meikle, W. P. S. 2008, A&A, 483, L47

Turatto, M., Cappellaro, E., Danziger, I. J. et al. 1993, MNRAS, 262, 128

Uomoto, A. 1986, ApJ, 310, L35

Valenti, S., Sand, D., Stritzinger, M. D. et al. MNRAS, 449, 2608

de Vaucouleurs, G., de Vaucouleurs, A., & Buta, R. 1981, PASP, 93, 36

Vink, J. S., de Koter, A., & Lamers, H. J. G. L. M. 2001, A&A, 369, 574

Wang, L., Baade, D., Höflich, P. et al. 2004, ApJ, 604, L53

Walborn, N. R., Lasker, B. M., Laidler, V. G., & Chu, Y.-H. 1987, ApJ, 321, L41

Weiler, K. W., Panagia, N., Sramek, R. A. et al. 1989, ApJ, 336, 421

Weiler, K. W., van Dyk, S. D., Discenna, J. L., Panagia, N., & Sramek, R. A. 1991, ApJ, 380, 161

Wheeler, J. C., Yi, I., Höflich, P., & Wang, L. 2000, ApJ, 537, 810

Whelan, J., & Iben, I. Jr. 1973, ApJ, 186, 1007

Williams, C. L., Panagia, N., van Dyk, S. D. et al. 2002, ApJ, 581, 396

Woosley, S. E. 1993, ApJ, 405, 273

Woosley, S. E., & Heger, A. 2007, Physics Reports, 442, 269

Woosley, S. E., Pinto, P. A., Martin, P. G., & Weaver, T. A. 1987, ApJ, 318, 664

Woosley, S. E., Blinnikov, S., & Heger, A. 2007, Nature, 450, 390

Yan, L., Quimby, R., Gal-Yam, A. et al. 2016, eprint arXiv:1611.02782, submitted to ApJ

Yoon, S.-C., Gräfener, G., Vink, J. S., Kozyreva, A., & Izzard, R. G. 2012, A&A, 544, L11

Yoon, S.-C., Dessart, L., & Clocchiatti, A. 2017, eprint arXiv:1701.02089, submitted to ApJ

Zaritsky, D., Kennicutt, R. C. Jr., & Huchra, J. P. 1994, ApJ, 420, 87

Zhang, T., Wang, X., Wu, C. et al. 2012, AJ, 144, 131

Annales Universitatis Turkuensis

Turun yliopisto
University of Turku

Painosalama Oy, Turku, Finland 2017

ISBN 978-951-29-6820-6 (PRINT)
ISBN 978-951-29-6821-3 (PDF)
ISSN 0082-7002 (Print) | ISSN 2343-3175 (Online)